

Streaming motions of galaxy clusters within 12000 km s^{-1} — V. The peculiar velocity field

Michael J. Hudson¹, Russell J. Smith¹, John R. Lucey² and Enzo Branchini³

¹ Department of Physics, University of Waterloo, Waterloo, Ontario N2L 3G1, Canada.

E-mail: mjhudson@uwaterloo.ca, rjsmith@astro.uwaterloo.ca

² Department of Physics, University of Durham, South Road, Durham DH1 3LE, United Kingdom. E-mail: John.Lucey@durham.ac.uk

³ Dipartimento di Fisica, Università degli Studi Roma TRE, Roma, Italia

11 December 2018

ABSTRACT

We analyze in detail the peculiar velocity field traced by 56 clusters within $120 h^{-1}\text{Mpc}$ in the “Streaming Motions of Abell Clusters” (SMAC) sample. The bulk flow of the SMAC sample is $687 \pm 203 \text{ km s}^{-1}$, toward $l = 260^\circ \pm 13^\circ$, $b = 0^\circ \pm 11^\circ$. We discuss possible systematic errors and show that no systematic effect is larger than half of the random error. The flow does not drop off significantly with depth, which suggests that it is generated by structures on large scales. In particular, a Great Attractor as originally proposed by Lynden-Bell et al. cannot be responsible for the SMAC bulk flow. The SMAC data suggest infall into an attractor at the location of the Shapley Concentration, but the detection is marginal (at the 90% confidence level). We find that distant attractors in addition to the Shapley Concentration are required to explain the SMAC bulk flow. A comparison with peculiar velocities predicted from the *IRAS* PSCz redshift survey shows good agreement with a best fit value of $\beta_1 = \Omega_m^{0.6}/b_1 = 0.39 \pm 0.17$. However, the PSCz density field is not sufficient to account for all of the SMAC bulk motion. We also detect, at the 98% confidence level, a residual bulk flow of $372 \pm 127 \text{ km s}^{-1}$ toward $l = 273^\circ$, $b = 6^\circ$ which must be generated by sources not included in the PSCz catalogue, that is, either beyond $200 h^{-1}\text{Mpc}$, in the Zone of Avoidance or in superclusters undersampled by *IRAS*. Finally, we compare the SMAC bulk flow with other recent measurements. We argue that, at depths ranging from 60 to $120 h^{-1}\text{Mpc}$, flows of order 600 km s^{-1} are excluded by multiple data sets. However, convergence to the CMB frame by a depth of $60 h^{-1}\text{Mpc}$ is also excluded by multiple data sets. We suggest that a bulk flow of 225 km s^{-1} toward $l = 300^\circ$, $b = 10^\circ$ at depths greater than $60 h^{-1}\text{Mpc}$ is consistent with all peculiar velocity surveys, when allowance is made for sparse sampling effects.

Key words: galaxies: distances and redshifts – galaxies: elliptical and lenticular, cD – galaxies: clusters: general – surveys – cosmological parameters – large-scale structure of Universe

1 INTRODUCTION

The source of the Local Group’s (LG) peculiar velocity of $627 \pm 22 \text{ km s}^{-1}$ toward $l = 276^\circ$, $b = 30^\circ$ (Kogut et al. 1993) with respect to the Cosmic Microwave Background (CMB) has been a puzzle since the detection of the CMB dipole (Smoot et al. 1977). In order to resolve this fundamental question, it is necessary to map the peculiar velocities of nearby galaxies. If a volume which is at rest with respect to the CMB can be identified, then the masses responsible for the motion of the LG must be contained within that volume.

An important milestone in peculiar velocity surveys was the study of Lynden-Bell et al. (1988), who used the $D_n - \sigma$ distance indicator and claimed detection of a “Great Attractor” (GA) at a distance of approximately $45 h^{-1}\text{Mpc}$ believed to be responsi-

ble for most the LG’s motion. Subsequent peculiar velocity surveys of the nearby Universe undertaken in the early 90s did not reveal the expected infall signature on the far side of the GA (Mathewson et al. 1992) and hinted at a large coherence length for the flow (Willick 1990; Courteau 1992). Analyses of redshift surveys (Dressler 1988; Strauss et al. 1992; Hudson 1993, 1994) did identify a significant excess of galaxies near the proposed GA, but with an abundance insufficient to generate the LG’s motion. For example, Hudson (1994) concluded that $400 \pm 45 \text{ km s}^{-1}$ of the LG’s motion arose from sources beyond $80 h^{-1}\text{Mpc}$. The location of the peak of the GA in the Zone of Avoidance (ZOA), as given by Kolatt et al. (1995), suggests the possibility that most of the GA’s overdensity may be obscured. Searches in the ZOA have revealed the presence of massive clusters such as A3627 (Kraan-Korteweg et al. 1996) but the integrated overdensity within

the ZOA appears still insufficient to generate substantial infall at the LG (Staveley-Smith et al. 2000).

Lauer & Postman (1994, hereafter LP) used the photometric properties of brightest cluster galaxies as standard candles and claimed that a much larger region of space extending to $150 h^{-1} \text{Mpc}$ was moving at a velocity of $689 \pm 178 \text{ km s}^{-1}$ toward $l = 343^\circ$, $b = 52^\circ$. The LP result was puzzling, first because the amplitude of the flow on such a large scale was higher than expected in popular cosmological models (Strauss et al. 1995), and second because the direction of the LP flow was significantly different from previous bulk flow measurements (Strauss & Willick 1995).

Recent surveys of field galaxies to depths $R \lesssim 60 h^{-1} \text{Mpc}$ generally suggest that the bulk flow within these nearby volumes is in the range from $100 - 300 \text{ km s}^{-1}$ in the direction $l \approx 300^\circ$, $b \approx 10^\circ$ (Willick et al. 1997; Giovanelli et al. 1998; Courteau et al. 2000; da Costa et al. 2000; Tonry et al. 2000). Clusters surveys on large ($R \gtrsim 100 h^{-1} \text{Mpc}$) scales have not supported the LP result, but, at face value, also appear to suggest a wide range of values for the large-scale motion (Mould et al. 1993; Hudson et al. 1999; Willick 1999; Dale et al. 1999; Colless et al. 2001). This apparent disagreement is due to neglect of sparse sampling on the quoted flow errors (Watkins & Feldman 1995). When the effects of sparse sampling are properly taken into account, the large-scale surveys are not in conflict (Hudson 2003). For recent reviews, the reader is directed to Courteau & Dekel (2001) and Zaroubi (2002).

This paper is the fifth in a series based on the ‘‘Streaming Motions of Abell Clusters’’ (SMAC) project. The aim of this project is to obtain distance estimates, via the Fundamental Plane (FP) method, for elliptical galaxies in clusters and to map the peculiar velocity field within $120 h^{-1} \text{Mpc}$ of the Local Group. First results from this work were presented in Hudson et al. (1999), who quoted a bulk flow of $630 \pm 200 \text{ km s}^{-1}$ toward $l = 260^\circ$, $b = -1^\circ$ from a preliminary analysis of the same sample studied here.

Previous papers in this series have reported new data for this project. Smith et al. (2000, 2001, hereafter SMAC-I and SMAC-II respectively) presented spectroscopic and photometric data, respectively; these data were compared and combined with other data available in the literature to obtain the final data set used for this project (Hudson et al. 2001, hereafter SMAC-III). Smith et al. (in preparation, hereafter SMAC-IV) reports FP distances for 56 clusters.

In this paper, we analyze the peculiar velocity field in the Universe as traced by the SMAC clusters. In Section 2, we summarize the SMAC peculiar velocity data. In Section 3, we model the peculiar velocity field as a simple bulk flow (the dipole moment of the velocity field). An important aspect of this paper is to evaluate the robustness of the results to systematic effects (Section 3.3). In Section 4 we consider more complicated flow models, including toy models based on simple attractors. Section 5 compares the peculiar velocities of SMAC clusters to the predictions from the *IRAS* PSCz density field. Section 6 compares the flow of the SMAC sample to other results in the literature.

2 DATA

In SMAC-IV, we tabulated peculiar velocity data for 56 clusters spanning the whole sky, and extending to a distance of $\sim 120 h^{-1} \text{Mpc}$. The peculiar velocities quoted there were based on an inverse fit to the FP, in which $\log \sigma$ is regressed on $\log R_e$ and $\langle \mu \rangle_e$.

The inverse fit has the advantage that it is insensitive to selection on the photometric parameters.

Median peculiar velocity errors per cluster are $\sim 575 \text{ km s}^{-1}$. These errors are primarily due to intrinsic scatter in the Fundamental Plane which contributes a fractional distance error of $0.21/\sqrt{N}$, where N is the number of galaxies in the cluster. However, the errors also include the effect of the 16% uncertainties in the Schlegel et al. (1998, hereafter SFD) extinctions and uncertainties in the mean redshifts of the clusters.

In SMAC-IV, we also quoted for each cluster the error contribution arising from uncertainties in matching velocity dispersions from disparate observing runs. An important aspect of this work is the treatment of these errors, which are not independent from cluster to cluster, but are correlated on the sky. To calculate their effect on the bulk flow, we bootstrap re-sample the ‘‘overlap’’ sample used to calculate the velocity dispersion matching corrections. We then generate new FP datasets using those bootstrapped corrections and use these bootstrap samples to calculate the covariance matrix of the cluster peculiar velocities. We find that these systematic errors do not dominate the error budget in the bulk flow. On the other hand, due to their coherent nature, neither can they be neglected (see Section 3.3.1 below).

3 THE BULK FLOW

3.1 Flow Model

One statistic of particular interest is the bulk flow, or the dipole moment of the peculiar velocity field. For an idealized densely-sampled survey, the bulk flow would reflect the gravitational pull of mass near to and beyond the survey limits. It is therefore sensitive to the distribution of mass on the largest scales.

We fit the radial components of the cluster peculiar velocities with the flow model

$$U(\mathbf{r}) = \mathbf{V} \cdot \hat{\mathbf{r}} + \frac{\Delta H}{H} r \quad (1)$$

where the free parameters are \mathbf{V} , the bulk flow vector, and $\Delta H/H$, a perturbation to the assumed Hubble constant. The distances quoted in SMAC-IV are in units of km s^{-1} and have already been adjusted so that the best fit gives $\Delta H = 0$, but leaving this parameter free allows for the correct propagation of errors into the bulk flow \mathbf{V} . We use Galactic coordinates as the basis for our Cartesian coordinates: z is toward the North Galactic Pole ($b = 90^\circ$), x is in the direction of the Galactic centre ($l = 0^\circ$), and y is in the direction of rotation ($l = 90^\circ$).

As noted above, the errors in the peculiar velocities are not independent but rather are coupled through the velocity-dispersion system-matching corrections described above and in Paper III. We construct a 56×56 covariance matrix which consists of the variance in distance due to scatter in the FP plus the square of a ‘‘thermal’’ scatter $\sigma_{\text{th}} = 250 \text{ km s}^{-1}$, where the latter term reflects the small-scale noise of individual clusters around the mean bulk flow. These errors are independent from cluster to cluster so this part of the covariance matrix is diagonal. This is then added to the system-matching covariance matrix to obtain the full covariance matrix, C . We then minimize

$$\chi^2 = \sum_{i,j} [u_i - U(\mathbf{r}_i)] [C^{-1}]_{ij} [u_j - U(\mathbf{r}_j)] \quad (2)$$

where the C^{-1} is the inverse covariance matrix.

To assess the depth of a sparse sample such as SMAC, we define an error-weighted effective depth,

$$R_* = \frac{\sum_i r_i / \sigma_i^2}{\sum_i 1 / \sigma_i^2} \quad (3)$$

where σ_i^2 are the peculiar velocity errors, i.e., the diagonal elements of C . For an idealized, densely-sampled survey filling a top-hat sphere of radius R with uniform distance errors for all objects, one would obtain $R_* = R/2$. With our choice of error weighting, the SMAC sample has $R_* \sim 6300 \text{ km s}^{-1}$, as expected for a survey extending to $\sim 12000 \text{ km s}^{-1}$.

3.2 Results

For our preferred choice $\sigma_{\text{th}} = 250 \text{ km s}^{-1}$, the SMAC bulk flow is $687 \pm 203 \text{ km s}^{-1}$, toward $l = 260^\circ \pm 13^\circ$, $b = 0^\circ \pm 11^\circ$. In Galactic Cartesian coordinates, this is $V_x = -124 \pm 172 \text{ km s}^{-1}$, $V_y = -676 \pm 190 \text{ km s}^{-1}$, $V_z = -5 \pm 131 \text{ km s}^{-1}$, and in Supergalactic Cartesian this becomes $V_{\text{SGX}} = -367 \text{ km s}^{-1}$, $V_{\text{SGY}} = 59 \text{ km s}^{-1}$, $V_{\text{SGZ}} = -578 \text{ km s}^{-1}$, in the direction $\text{SGL} = 171^\circ$, $\text{SGB} = -57^\circ$. This flow is significantly different from zero at the 99.91% confidence level (CL). In some papers (Lauer & Postman 1994, including Hudson et al. 1999), the authors allow for “error-bias”. This is a bias which arises because the bulk flow amplitude is the square root of the quadrature sum of vector components and so is a positive definite quantity. Even if the true bulk flow were zero, random errors in the components would yield a positive amplitude bulk flow. For the same reasons, in the more general case of a non-zero bulk flow, random errors bias the amplitude high. The “error-bias corrected” value of the SMAC bulk flow is 620 km s^{-1} .

Fig. 1 shows a “tadpole diagram” of the SMAC data projected onto a plane in which the negative X-axis is along the direction of the SMAC bulk flow and the vertical axis points to the Galactic poles. Note the excess of outflowing clusters on the left-hand side and the inflowing clusters on the right-hand side, the signature of a bulk flow. In contrast, the objects at the top and bottom scatter around zero peculiar velocity. The bulk flow has a negligible component in the vertical (NGP/SGP) direction. Fig. 2 shows the SMAC data in four different planes rotated by 45° around the SGY axis. Panel (a) corresponds to the Supergalactic Plane. Panel (b) is closest to the plane of the SMAC flow.

It is difficult to illustrate the peculiar velocity errors in tadpole diagrams. Fig. 3 shows four Monte Carlo realizations of the peculiar velocity field where we perturb the observed distances around their measured values with a Gaussian random error. Robust regions of the peculiar velocity field include the clump of positive peculiar velocities in the top left quadrant and the negative peculiar velocities in the distant part of the bottom right quadrant.

The bulk flow errors quoted above are marginal errors, i.e. they are the diagonal elements of the covariance matrix. The error covariance matrix is not isotropic; it is a triaxial ellipsoid. The long axis of the error ellipsoid is oriented toward $l = 223^\circ$, $b = -10^\circ$ (and its antipode). The error along this direction is 222 km s^{-1} . The intermediate axis is toward $l = 332^\circ$, $b = -41^\circ$, and the error is 152 km s^{-1} . The error along the short axis is 102 km s^{-1} . The corresponding direction (toward $l = 312^\circ$, $b = 46^\circ$) is the direction along which the bulk flow is most precisely measured. Because the SMAC sample has good sky coverage, the bulk flow is almost independent of the monopole ($\Delta H/H$) term: the correlation coefficient between it and the bulk flow amplitude is only 0.09.

We find that the recovered SMAC bulk flow depends very weakly on the value of σ_{th} . If we fit for σ_{th} we find $\sigma_{\text{th}} = 190 \pm 105 \text{ km s}^{-1}$. For $\sigma_{\text{th}} = 190 \text{ km s}^{-1}$, the bulk flow is only 16 km s^{-1} lower than for the default $\sigma_{\text{th}} = 250 \text{ km s}^{-1}$ case.

The flow therefore appears to be quite cold, i.e. the bulk flow dominates over small-scale “thermal” motions of clusters. The cosmic Mach number (Ostriker & Suto 1990) is the ratio of the bulk flow velocity of a volume to the 3D velocity dispersion of the objects in the frame of the mean motion, $\mathcal{M} = |V|/(\sqrt{3}\sigma_{\text{th}})$. For the SMAC sample, we find $\mathcal{M} = 2.0 \pm 1.3$. The errors on this quantity are obtained by propagation of errors, a procedure not strictly valid given the size of the errors in comparison to the measurement.

To test the coherence of the bulk flow, we have divided the sample into statistically-independent nearby ($z_c < 7500 \text{ km s}^{-1}$, with an effective depth $R_* = 50h^{-1} \text{ Mpc}$) and a distant subsamples ($z_c > 7500 \text{ km s}^{-1}$, with $R_* = 98h^{-1} \text{ Mpc}$). The nearby sample has a bulk flow of $640 \pm 290 \text{ km s}^{-1}$ toward $l = 266^\circ$, $b = -17^\circ$. This is significantly different from 0 at the 97% confidence level. At this depth, flows of order several hundred km s^{-1} are known to exist (Courteau & Dekel 2001; Zaroubi 2002), and the SMAC result is consistent with these. The distant subsample yields a somewhat larger bulk flow ($975 \pm 300 \text{ km s}^{-1}$ toward $l = 267^\circ$, $b = 16^\circ$). Although the errors are large, the bulk flow of the distant subsample is significantly different from zero at the 99.5% confidence level. It is not statistically different from the bulk flow of the nearby subsample. Fig. 4 shows the components of the bulk flow for nearby and distant subsamples separated at different values of R . At no value of R are the bulk flows of the two subsamples inconsistent. This coherence suggests that there are significant contributions to peculiar velocities in the nearby Universe arising from density fluctuations on very large ($\sim 100h^{-1} \text{ Mpc}$) scales.

3.3 Possible Sources of Systematic Error

In this section, we examine possible systematics and assess the robustness of the bulk flow. There are many sources of error that could affect a cluster’s peculiar velocity, but in general such errors will only increase the scatter in the FP or add a random error to the cluster peculiar velocities. The bulk flow is the dipole of the peculiar velocity field, so in order for it to be affected by a systematic error, the systematic error must be coherent over large areas of sky. The most likely sources of such an effect are problems matching data from different observing runs, or systematic errors in Galactic extinction corrections.

3.3.1 Spectroscopic Data

Systematic errors in velocity dispersion measurements could, in principle, lead to large errors in the bulk flow. For example, if velocity dispersions measured in the North were systematically 1% smaller than those measured in the South, then distances in the North would be too short by 1.4%. For the SMAC sample, this would yield a spurious bulk flow of $\sim 50 \text{ km s}^{-1}$ toward the North Celestial Pole. Because of these possible effects, great care was taken to obtain comparison data for the same objects from multiple telescopes (SMAC-I). In SMAC-III, we calculated the corrections required for each run as well as the correlated uncertainties in these corrections. The latter are fully propagated to the bulk flow and are thus included in the error covariance matrix appearing in Equation (2). Because of the large number of comparison data, these errors do not dominate the error in the bulk flow: had we neglected

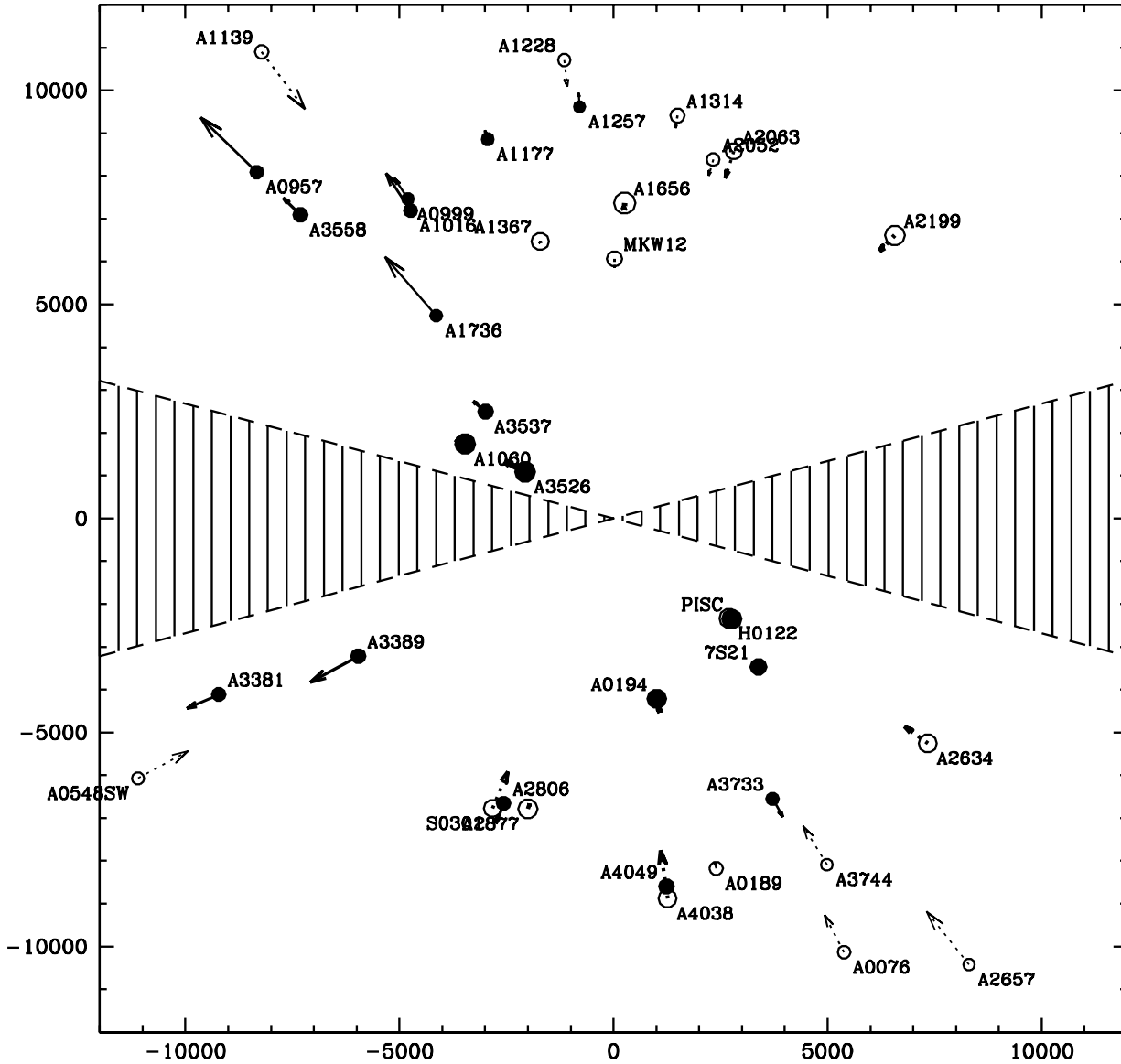


Figure 1. Peculiar velocities of SMAC clusters projected onto a plane in which the negative X-axis is along the direction of the SMAC bulk flow and the vertical axis points to the Galactic poles. Clusters within $\pm 45^\circ$ of the plane are plotted. The circle indicates the estimated distance to the cluster, projected onto the plane, and the end of the tail is at the CMB-frame cz , so the peculiar velocity is indicated in km s^{-1} by the length of the tail. Clusters with peculiar velocities away from the origin are filled circles with solid tails, whereas clusters with peculiar velocities toward the origin are shown as open circles and dotted tails. The size of the circle scales inversely with the distance errors. The hatched region indicates the Zone of Avoidance ($|b| < 20^\circ$).

these, we would have quoted an error of 188 km s^{-1} (compare with the correct value of 203 km s^{-1}). Subtracting these in quadrature, we can quantify the error in the bulk flow from system-matching uncertainties: 76 km s^{-1} .

In order to examine in more detail the effects of individual spectroscopic datasets, we have performed a “jackknife” test in which we exclude each dataset in turn, and recalculate the bulk flow. Some clusters, however, were observed only in one run, so the jackknife removes entire clusters from the sample and conse-

quently changes the spatial sampling of the survey. The results of this test are shown in Fig. 5. No single spectroscopic dataset has an effect on the bulk flow at a level of more than 70 km s^{-1} .

We conclude that errors in spectroscopic systems are fully quantified and controlled in the SMAC sample.

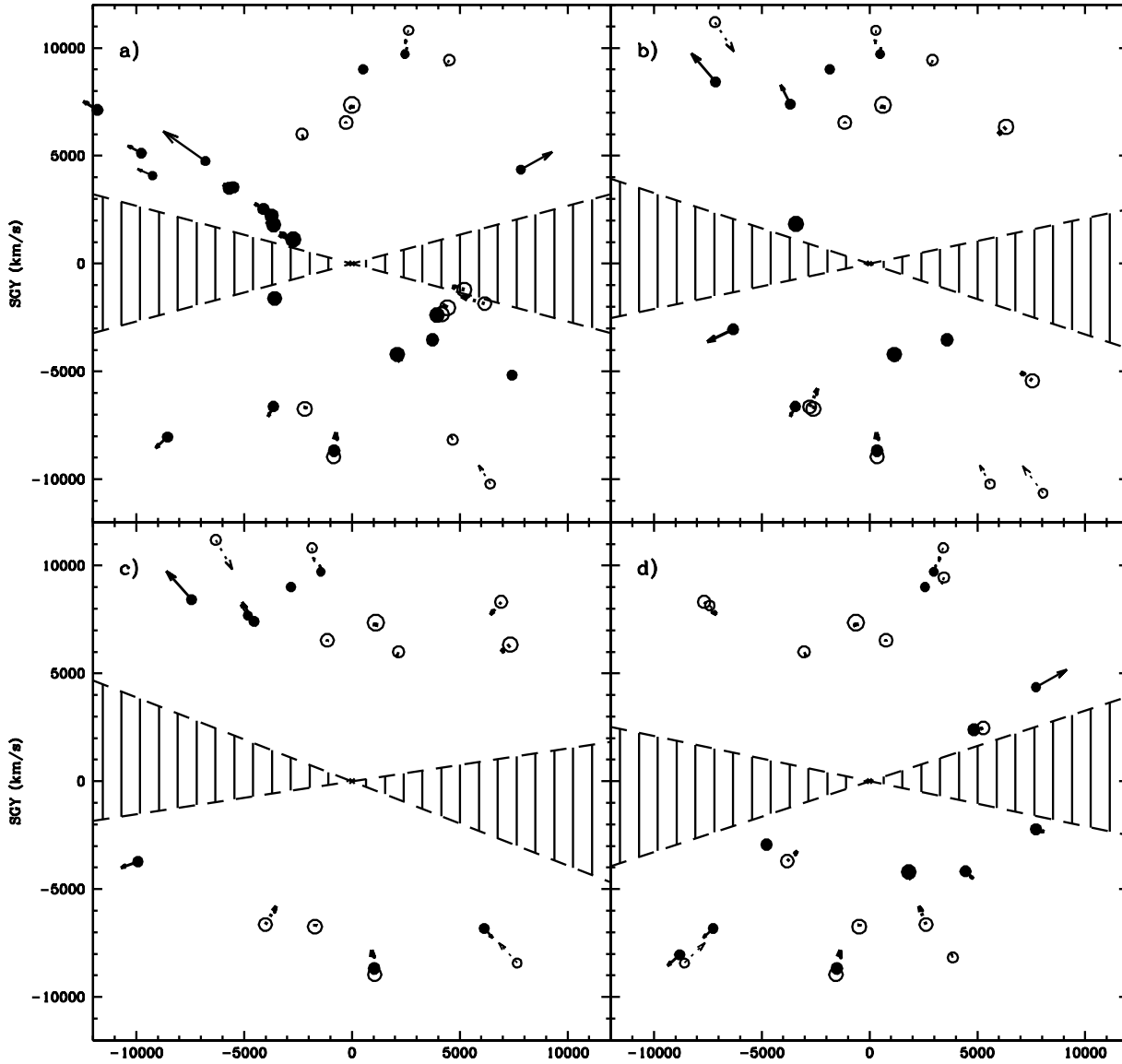


Figure 2. Peculiar velocities of SMAC clusters with symbols as in Fig. 1. Four planes are shown: (a) the Supergalactic Plane; (b) a plane rotated by 45° from the Supergalactic plane around the the SGY axis. The horizontal axis is $1/\sqrt{2} \text{ SGX} + 1/\sqrt{2} \text{ SGZ}$ (toward $\text{SGL}= 0, \text{SGB}= 45^\circ$). The SMAC flow is only 13° from this axis. The signature of a bulk flow, namely infalling objects on one half of the plot and outflowing ones on the other, is clearly seen in this panel. c) The $\text{SGX}=0$ plane d) a plane rotated a further 45° so that the horizontal axis is $1/\sqrt{2} \text{ SGX} - 1/\sqrt{2} \text{ SGZ}$. Only clusters within $\pm 22.5^\circ$ of the plane are plotted.

3.3.2 Extinction Corrections

The proximity of the SMAC flow to the Galactic plane suggests that errors in the extinction corrections could affect the bulk flow. In this subsection, we investigate the effects of extinction on the SMAC sample. Note that errors in distance due to random errors in extinction are included in the peculiar velocity errors tabulated in SMAC-IV, by assuming that the SFD extinctions are accurate to 16%. This error is applied to the cluster as whole rather than to indi-

vidual galaxies within the cluster, but is assumed to be independent from cluster to cluster. Extinction errors would have the greatest effect on clusters with the highest extinction. In the SMAC sample, there are 7 clusters (A0400, A0539, A0426, J8, A2657, A3526, A3733) with mean $E(B - V) > 0.1$ mag. and hence $A_R > 0.26$ mag. We find, however, that when these 7 clusters are excluded, the bulk flow drops by only 35 km s^{-1} . Thus the SMAC bulk flow is not substantially affected by random extinction errors.

Of greater concern is the possibility of coherent errors in the

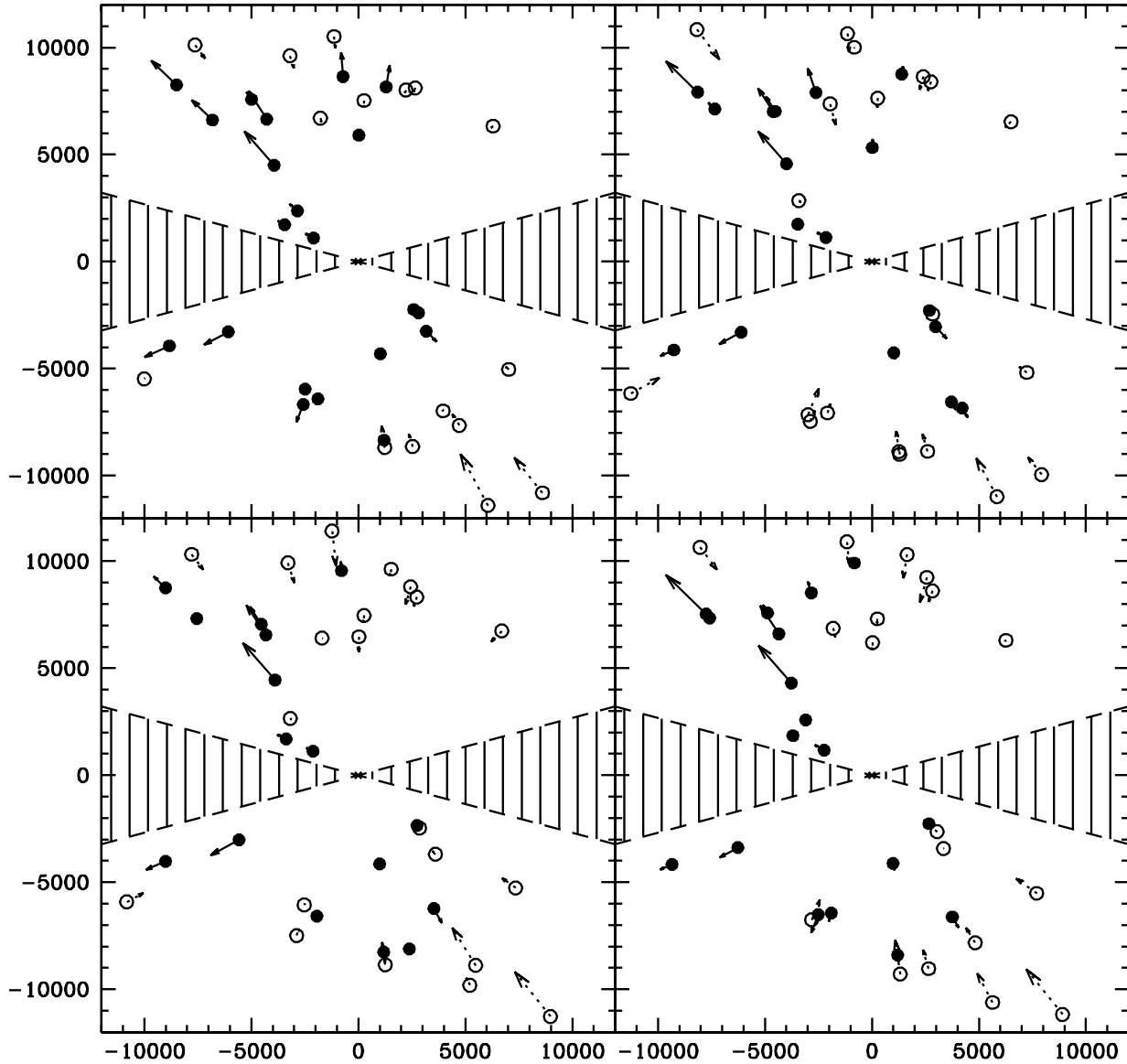


Figure 3. As in Fig. 1, but showing Monte Carlo realizations of the SMAC peculiar velocity field where we have perturbed the observed distances around their measured values according to their errors. Notice that the outflow pattern on the left hand side and the inflow pattern in the lower right corner are robust to random errors.

SFD maps. Hudson (1999) tested the SFD maps using data for early-type galaxies, which have a tight intrinsic $(B - V) - \text{Mg}_2$ relation, from Faber et al. (1989). He found no strong evidence for systematic dipolar errors in the SFD maps, and set an upper limit of 16% to such systematic errors. Blakeslee et al. (2001), using the $(V - I) - \text{Mg}_2$ relation also found no evidence of a systematic dipole error.

As a further test of systematic extinction errors, we have re-computed peculiar velocities and bulk flows using the extinction maps of Burstein & Heiles (1982, hereafter BH) in place of those of SFD. It is worth noting that the BH corrections yield

some anomalously large peculiar velocities. For example, A2634 has a peculiar velocity of $-1200 \pm 390 \text{ km s}^{-1}$ with the BH corrections, whereas with the SFD corrections its peculiar velocity is $-710 \pm 370 \text{ km s}^{-1}$. Similarly, the peculiar velocity of A2657 is $-3200 \pm 1200 \text{ km s}^{-1}$ with the BH corrections, and $-1600 \pm 1200 \text{ km s}^{-1}$ with the SFD corrections. Using the BH corrections, we obtain a bulk flow of 592 km s^{-1} , a reduction of 95 km s^{-1} compared with the result obtained with the SFD corrections. Thus uncertainties in Galactic extinction appear to affect the bulk flow at a level less than half the random error.

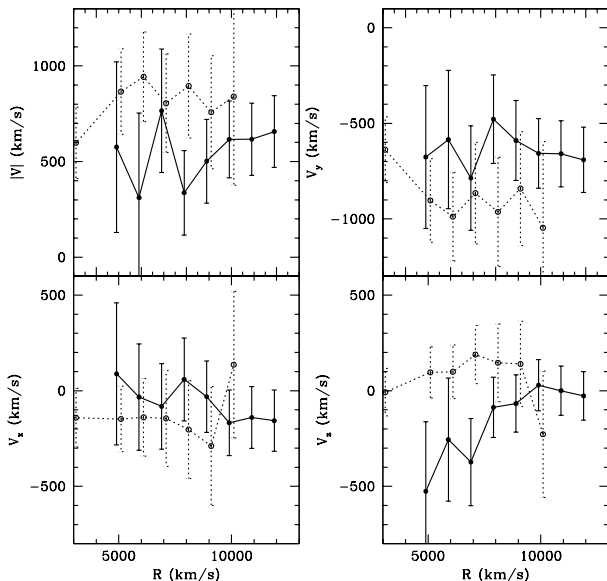


Figure 4. Bulk flow for different subsamples of the SMAC data selected by distance. Solid curves indicate subsamples with data in an inner sphere extending from the LG out to R . Dotted curves show bulk flows of subsamples in an outer shell extending from radius R to the edge of the SMAC sample. For clarity, the curves are offset slightly in the horizontal direction. For a given curve, the data points at different R are not independent, but at each R , the two subsamples are statistically independent. In all cases, the bulk flows of inner and outer samples are consistent with each other.

3.3.3 Stellar Populations

Variations in age and metallicity will introduce extra scatter in the FP. If there are systematic differences from cluster-to-cluster, then it is possible that the cluster peculiar velocities could be significantly in error. Mg_2 can serve as an indicator of age and/or metallicity. For example, the models of Worthey (1994) indicate that, for a typical elliptical, a -0.15 change in metallicity at solar abundance yields a Mg_2 change of -0.03 and an R-band change of -0.13 mag. Similarly if we add a 0.10 mass fraction in the form of an intermediate-age (5 Gyr) population, Mg_2 changes by -0.0083 mag, and R-band light changes by -0.10 mag.

In SMAC-IV, we compared residuals from the Mg_2 - σ relation with residuals from the inverse FP on a cluster-by-cluster basis and found no strong evidence for a correlation.

We also showed, however, that the FP- Mg_2 relation, which includes Mg_2 as a parameter in addition to the usual 3 FP parameters, does reduce the scatter in $\log \sigma$ in the inverse FP. We prefer not to use the FP- Mg_2 relation for our default solution for two reasons: first, Mg_2 is not available for all of our galaxies, and second, the scatter in *distance* for the FP- Mg_2 relation is actually larger than for the inverse FP, because the $\log R_e$ coefficient in the FP- Mg_2 relation differs from that of the FP relation. Nevertheless, if there are systematic variations from cluster-to-cluster, these can be corrected by including Mg_2 in the distance indicator. However, when we compare the same sample of clusters, we find that including the Mg_2 term increases the bulk flow by 261 km s^{-1} to 831 km s^{-1} towards lb254-7, while also increasing the error in the bulk flow to 230 km s^{-1} .

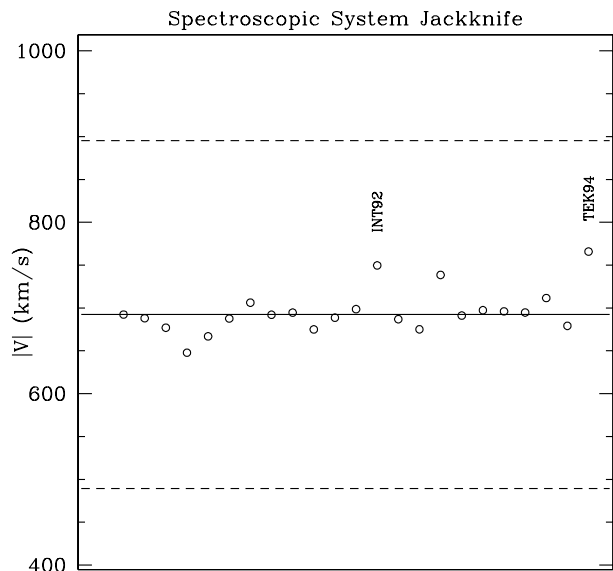


Figure 5. The jackknife test applied to the bulk flow statistic showing the effect of excluding a given spectroscopic run from the full solution. The vertical axis shows the amplitude of the bulk flow and the horizontal axis indexes different spectroscopic runs. Open circles show results for each spectroscopic run in turn. Those runs whose exclusion changes the bulk flow by more than 50 km s^{-1} are labelled. For details of the labels, see Smith et al. (2000). The solid line shows the best fit result from the whole sample, and the dashed lines show the 1σ errors on the amplitude. No individual spectroscopic run has a significant effect on the bulk flow.

3.3.4 Morphological Mix

The SMAC sample contains both E and S0 galaxies. In Hudson et al. (1997, hereafter PP-II), we compared the FP relations of E ($T \leq -4$) to S0 ($T \geq -3$) types. There we found a small and marginally significant (2σ) offset in the zero-point, in the sense that E types are observed to have larger velocity dispersions than S0 galaxies at fixed R_e and $\langle \mu \rangle_e$. Blakeslee et al. (2002) also noted differences between E and S0 in their comparison of FP and Surface Brightness Fluctuation (SBF) distances. In SMAC-IV, we repeated this analysis, this time with a free coefficient of the RC3 T -type. There we found a small and marginally significant correction to the FP predicted velocity dispersions (-0.0043 ± 0.0019 in $\log \sigma$ per unit of T -type). This corresponds to E types having $2.7 \pm 1.3\%$ larger velocity dispersions at a given R_e and $\langle \mu \rangle_e$ than S0 galaxies. This difference is smaller than, but consistent with, the offset found in PP-II. We have not included this term in our default solution because we do not expect any significant difference in the ratio of Es to S0s across the sky. When the term is included, the bulk flow drops by only $\sim 30 \text{ km s}^{-1}$. If we treat E and S0 subsamples separately, they both give a consistent bulk flow, the E sample of 417 galaxies yields a slightly lower amplitude ($601 \pm 195 \text{ km s}^{-1}$) bulk flow than the S0 sample of 277 galaxies ($762 \pm 294 \text{ km s}^{-1}$). The larger bulk flow error for the S0-only sample arises partly from the smaller number of galaxies in the S0 sample, and partly from the larger scatter in the S0 FP relation.

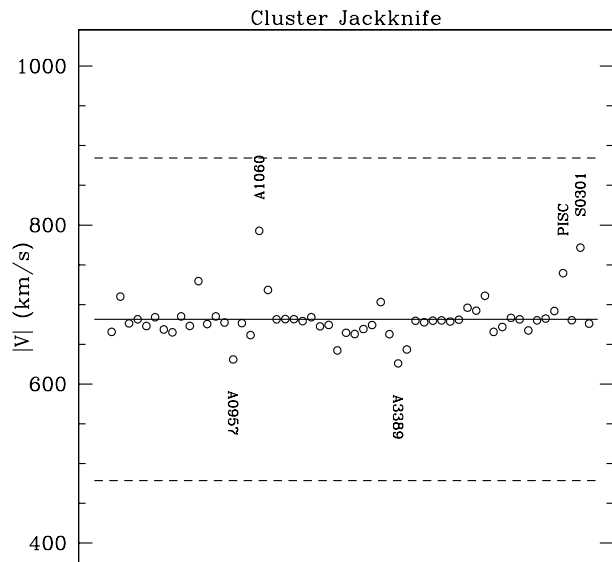


Figure 6. As in Fig. 5, but showing the effect of excluding individual clusters of galaxies.

3.3.5 Outlying Data

In SMAC-IV, we removed 5 galaxies which deviated by more than 3 sigma from the best-fitting FP. Re-including these 5 outliers reduces the bulk flow by 56 km s^{-1} .

In Fig. 6, we show the effect on the bulk flow amplitude of removing entire clusters. Clusters which affect the bulk flow more than most are indicated. No single cluster influences the bulk flow upwards by more than 55 km s^{-1} . In particular, removing the nearby Centaurus cluster (which includes both the Cen30 and Cen45 sub-components) has little impact on the bulk flow (reducing it by only 40 km s^{-1}).

Gibbons et al. (2001) have suggested that FP clusters with large internal FP scatter have significantly larger peculiar velocity amplitudes. This might arise, for example, in cases where it is difficult to separate double clusters in which the two components are superimposed along the line of sight but are at slightly different distances. The spread of distances would then be increased, and the mean distance, and hence peculiar velocity, would be more susceptible to how the two components are sampled. Classic cases where this situation occurs are Abell 400 and Cen30/45. We examined this issue in Paper IV and found no strong evidence for a difference between the peculiar velocities of high and low scatter clusters.

Despite our non-detection of this effect, we have experimented with a weighting scheme in which the error for each cluster’s distance is based on the FP scatter for that cluster, rather than a global value. This procedure down-weights those clusters with large internal scatter. When we apply this weighting scheme, we find that the bulk flow drops, but only by $\sim 80 \text{ km s}^{-1}$.

3.3.6 Malmquist Bias Corrections

The procedure we have followed involves first calculating cluster distances from the inverse FP and then fitting these to a flow model. In the terminology of Strauss & Willick (1995), this is “Method I”. In this method, the estimate of each cluster’s distance is its inverse

FP distances (as opposed to its redshift), and so these distances must be corrected for Malmquist bias. One advantage of working with clusters is that this correction is small, since it scales as the inverse of the number of objects in the cluster.

It is also possible to fit the flow model and FP relation simultaneously. In this alternative “Method II” fit, redshift (corrected by the flow model) is the *a priori* distance indicator. As a result, no Malmquist bias corrections are necessary¹. A Method II analysis of the SMAC sample assuming a simple bulk flow model yields a bulk flow amplitude only $\sim 20 \text{ km s}^{-1}$ less than our standard result with Malmquist bias corrections, indicating that the details of Malmquist bias correction have little effect on the bulk flow.

3.3.7 Summary of Systematic Effects

We have examined several possible sources of systematic error. The most obvious source of systematic error, namely mismatches between velocity dispersions obtained on different runs is fully accounted for in our standard error analysis. The only systematic effect which might reduce the bulk flow is using the BH extinction maps (at the price of introducing very large peculiar velocities for two clusters). This would lower the flow by less than 100 km s^{-1} . Thus systematic errors in the bulk flow appear to be negligible in comparison to the random error of $\sim 200 \text{ km s}^{-1}$.

4 OTHER FLOW MODELS

4.1 Hubble Bubble

Zehavi et al. (1998), in an analysis of 44 SNIa distances, claimed evidence for a “Hubble bubble”, i.e. that the local Universe within 7000 km s^{-1} is underdense with the result that the local value Hubble constant is too high compared to the global value, $\Delta H/H = 6.5 \pm 2.2\%$. Giovanelli et al. (1999), using the TF relation, found a statistically insignificant “bubble” of $\Delta H/H = 1 \pm 2\%$.

We have tested this model with the SMAC data. We measure a local Hubble bubble of $2.3 \pm 1.9\%$ within the same distance studied by Zehavi et al. This result is consistent with zero. However, allowing for errors in the Zehavi et al. result as well as ours, the two results are consistent. We do not find any evidence of a Hubble bubble if we cut the SMAC sample at other radii. Taking all of these results at face value suggests there is at most a modest Hubble bubble with $\Delta H/H \sim 3 \pm 1.3\%$.

4.2 Bulk Flow plus Shear

The large scale shear of the peculiar velocity field offers an opportunity to identify the distances of the sources responsible for the bulk flow (Lilje et al. 1986) particularly if they are near the survey limits or in the Zone of Avoidance. For example, if there were an attractor just beyond the SMAC survey limits, then, relative to a pure bulk flow, the peculiar velocities would be more positive at the edge close to the attractor and less negative on the opposite side of the sky. Thus the residuals from the constant bulk flow would have a tidal pattern, which might be measurable. Since the strength of the tidal field is inversely proportional to distance cubed, then if the attractor was very far distant, the measured shear would be small.

¹ Technically, there is a Malmquist-like bias associated with the error in the estimated redshift, but at the distances considered in this paper, this bias is very small.

To measure the shear, we modify equation (1) as follows:

$$U(\mathbf{r}) = \mathbf{V} \cdot \hat{\mathbf{r}} + \hat{\mathbf{r}} \cdot \mathbf{h} \cdot \mathbf{r} \quad (4)$$

where \mathbf{h} is a symmetric shear tensor. The shear tensor measures anisotropies in the Hubble expansion. When the shear tensor is diagonalized, each eigenvalue corresponds to the difference in the expansion rate ($\Delta H/H$) along the corresponding eigenaxis. This differs from equation (1) where the Hubble constant was allowed to float, but was forced to be the same in all directions.

When this fit is performed, we find no significant reduction in χ^2 compared with bulk flow only fits. The direction of expansion ($6 \pm 3\%$) is towards $l = 315^\circ$, $b = -7^\circ$ and its antipole. The direction of expansion is very close to the negative SGY axis in the Supergalactic Plane. The direction of compression ($5.5 \pm 3\%$) is towards $l = 208^\circ$, $b = -68^\circ$ and antipole. However, these amplitudes are not statistically significant, and consequently the directions of expansion and compression are ill-defined due to the large errors. With this fit, the bulk flow is essentially unchanged: we find $615 \pm 211 \text{ km s}^{-1}$ toward $l = 259^\circ$, $b = 4^\circ$.

4.3 Attractor Models

Next we consider models with simple attractors. Although such models are likely to be only a crude approximation to a Gaussian random density field, they allow us to gain some insight into cosmographical features in the nearby Universe. The SMAC cluster data are rather sparse so we do not attempt to identify attractors in the data themselves. Instead we concentrate on attractor models using distances and profiles fixed by other authors.

We model the radial infall component towards an attractor with the following functional form:

$$u_a(\mathbf{r}) = \left(v_a \frac{r_a}{d_a} \left[\frac{(d_a^2 + c_a^2)}{(r_a^2 + c_a^2)} \right]^{(n_a+1)/2} \right) \cdot \hat{\mathbf{r}}, \quad (5)$$

where d_a is the distance from the LG to the attractor, $\mathbf{r}_a = \mathbf{d}_a - \mathbf{r}$ is the vector from the point \mathbf{r} to the centre of the attractor, c_a is a core radius and v_a is the velocity infall towards the attractor at the position of the LG. The infall is $u_a \sim 0$ at $r_a \sim 0$, peaks near $r_a \sim c_a$ and then falls off as $u_a \sim r_a^{-n_a}$ at large r_a . Here we fix $n_a = 2$.

The first attractor we consider is the ‘‘Great Attractor’’, using the flow model of Faber and Burstein (1988, hereafter FB88), except that for simplicity we use $n_a = 2$ rather than $n_a = 1.7$ adopted by FB88. We keep the location ($r_{GA} = 4200 \text{ km s}^{-1}$ in the direction $l = 309^\circ$, $b = 18^\circ$) and core radius (1400 km s^{-1}) of this attractor fixed with the parameters in the FB88 model, and fit only for one free parameter: the infall towards the GA at distance of the LG. With no bulk flow in the fit, the infall from the GA is $88 \pm 68 \text{ km s}^{-1}$. This is consistent with zero and differs significantly from the result of FB88 who found $v_{GA} = 535 \text{ km s}^{-1}$. Note that in Fig. 2a, there is no evidence of infall into the GA on its far side. We caution, however, that our data are sparse in the immediate vicinity of the GA. There are only three SMAC clusters for which the FB88 GA model predicts significant negative peculiar velocities ($u_{GA} < -500 \text{ km s}^{-1}$). For each of these three clusters, the SMAC peculiar velocity is positive. If we include a bulk flow in the fits, the GA infall is even smaller ($13 \pm 70 \text{ km s}^{-1}$). These conclusions do not change if we adopt the GA position of Kolatt et al. (1995). We conclude that there is little evidence from our sample for a very large mass at the position of the GA. However, it should

be noted that the errors are large: the 95% upper limit from our bulk flow plus GA model is $v_{GA} \sim 150 \text{ km s}^{-1}$.

Hudson (1993), in his analysis of the density field of optically-selected galaxies, found the GA overdensity was better described as a broad overdensity centred on the Centaurus cluster. He predicted an infall of $287 \pm 62 \text{ km s}^{-1}$ at the LG for $\beta_{opt} = 0.5$. In their analysis of SBF data, Tonry et al. (2000) fitted a ‘‘GA’’ model, the centre of which is almost coincident with Centaurus cluster. They obtained an infall of $289 \pm 137 \text{ km s}^{-1}$ at the LG, in good agreement with the Hudson (1993) prediction. If we adopt the GA/Centaurus attractor centre of Tonry et al. (2000), we find an infall of $58 \pm 153 \text{ km s}^{-1}$. It is difficult to make an exact comparison because the details of the infall model of Tonry et al. (2000) is different from ours, but our results do not appear to be in conflict with theirs.

It is clear that local ($R < 60h^{-1} \text{ Mpc}$) attractors are not responsible for the large-scale flow seen in the SMAC sample. The sample must be responding to sources at distances beyond the SMAC effective depth of 6000 km s^{-1} . The next attractor considered is the Shapley Concentration (SC) centered on the rich cluster Abell 3558 at $l = 312^\circ$, $b = 31^\circ$ and a distance of $145 h^{-1} \text{ Mpc}$. Since there are SMAC clusters quite close to the SC, it is important to model the SC as an extended mass distribution. The model given by equation (5) allows for a core radius of the attractor. The SC core radius is not well determined by the SMAC data themselves (a fit yields $\sim 30 \pm 20h^{-1} \text{ Mpc}$) so we fix it at $30 h^{-1} \text{ Mpc}$.

If we fit for only a SC attractor with no bulk flow, we find an infall at the LG of $200 \pm 60 \text{ km s}^{-1}$. This corresponds to an excess mass of $9 \pm 3 \times 10^{16} (\Omega_m/0.3)^{0.4} h^{-1} M_\odot$ from the SC region.

If we fit for the SC attractor plus a bulk flow, the infall due to the SC reduces to $140 \pm 80 \text{ km s}^{-1}$, and so is not statistically significant. For this model, the bulk flow is $620 \pm 220 \text{ km s}^{-1}$ and the direction has swung around by $\sim 10 \text{ deg}$ to $l = 248^\circ$, $b = -6^\circ$. This bulk flow is inconsistent with zero at the 95% CL. Note that there is strong covariance between the SC infall and the bulk flow which boosts both of their marginalized errors.

We conclude that there is a tantalizing suggestion for substantial mass at the SC, but that it is not the sole source of the SMAC bulk velocity.

5 THE PECULIAR VELOCITY FIELD PREDICTED BY THE IRAS PSCZ SURVEY

5.1 Method

The toy attractor models discussed above are rather crude. A better approach to modeling the peculiar velocity field is to use a redshift survey to reconstruct the real space density field of galaxies. If mass density contrasts are related to galaxy number-density contrasts according to a simple biasing relation, e.g. $\delta_g = b\delta$, then we can obtain predictions for the peculiar velocity field using the linear theory equation

$$\mathbf{u}_{lin}(\mathbf{r}) = \frac{\beta}{4\pi} \int \delta_g(\mathbf{r}') \frac{\mathbf{r}' - \mathbf{r}}{|\mathbf{r}' - \mathbf{r}|^3} d^3\mathbf{r}', \quad (6)$$

where $\beta = \Omega_m^{0.6}/b$. This method has been used by a number of workers to compare observed and predicted peculiar velocities and hence obtain β (see reviews by Strauss & Willick (1995), Courteau & Dekel (2001) and Zaroubi (2002)). For predictions of the peculiar velocities of clusters of galaxies, linear theory is adequate.

While the integral in equation (6) extends over all space, in practice, redshift surveys typically do not have data in the Zone of

Avoidance and are truncated at large distances where the corrections for selection effects become large. In the case of a distance-limited redshift survey, equation (6) then yields peculiar velocities in the frame of the center of mass of the redshift survey volume. In general, there will be contributions to the CMB-frame peculiar velocity from sources outside the redshift survey volume. If the redshift survey is much deeper than the peculiar velocity survey, and there are no massive structures in the ZOA, then the tidal or quadrupole effect from distant attractors, which falls as r^{-3} , will be small. It is then sufficient to model these residual contributions by adding a simple dipole term \mathbf{V}_{ext} to equation (6):

$$\mathbf{u}(\mathbf{r}) = \mathbf{u}_{\text{lin}}(\mathbf{r}) + \mathbf{V}_{\text{ext}} \cdot \hat{\mathbf{r}}. \quad (7)$$

There are several approaches to fitting β . One common approach is to perform the comparison between predicted and observed peculiar velocities in the LG frame. In this comparison, the exterior dipole cancels from the predictions since $\mathbf{u}_{\text{LG}}(\mathbf{r}) = \mathbf{u}(\mathbf{r}) - \mathbf{u}(0)$. An alternative approach is to fit in the CMB frame, but this ignores the LG as a data point entirely.

In this paper, we make the comparison in the CMB frame but we force our solutions to be consistent with the LG’s peculiar velocity. We implement this by including the three Cartesian components of the LG’s peculiar velocity as if they were three additional peculiar velocity data with zero observational error. We do, however, allow both the LG peculiar velocity components and the peculiar velocities of the SMAC clusters to have a random “thermal” component to their error. In this context, the “thermal” component represents the combined effects of non-linearities in the peculiar velocity field and errors in the peculiar velocities predicted from the galaxy density field.

5.2 Application to PSCz

For the galaxy redshift survey, we have used the *IRAS* Point Source Catalogue Redshift (PSCz) survey (Saunders et al. 2000b) with peculiar velocity predictions from Branchini et al. (1999). The distance limit of the density field is 20000 km/s. The Galactic Plane ($|b| < 8^\circ$) is filled by interpolating the data at higher $|b|$. The “real space” distances are obtained in a self-consistent way by an iterative method (see Branchini et al. (1999) for additional details).

The flow model uses equation (7) where \mathbf{u}_{lin} are the *IRAS* predictions, obtained by using the *IRAS* galaxy density field as δ_{g} in equation (6). This model has four free parameters: β_{I} and the three components of the \mathbf{V}_{ext} . We set the $\sigma_{\text{th}} = 150 \text{ km s}^{-1}$ for this comparison.

One final correction is necessary. We are making predictions for clusters of galaxies, which are significant mass concentrations. In the *IRAS* density field, these clusters will be located at a given “real-space” position as obtained by the self-consistent iterative reconstruction method. Due to distance errors, the observed SMAC cluster will, in general, be located a different distance along the line of sight from the *IRAS* cluster. We do not want the *IRAS* cluster to generate a spurious peculiar velocity at the location of the SMAC cluster, so for each SMAC cluster we identify and temporarily delete its counterpart in the *IRAS* density field before calculating the predicted peculiar velocity.

5.3 Results

Simultaneous fits of the parameters in equation (7) are given in Table 1. The best fit has $\beta_{\text{I}} = 0.39 \pm 0.17$ and $\mathbf{V}_{\text{ext}} = 372 \pm$

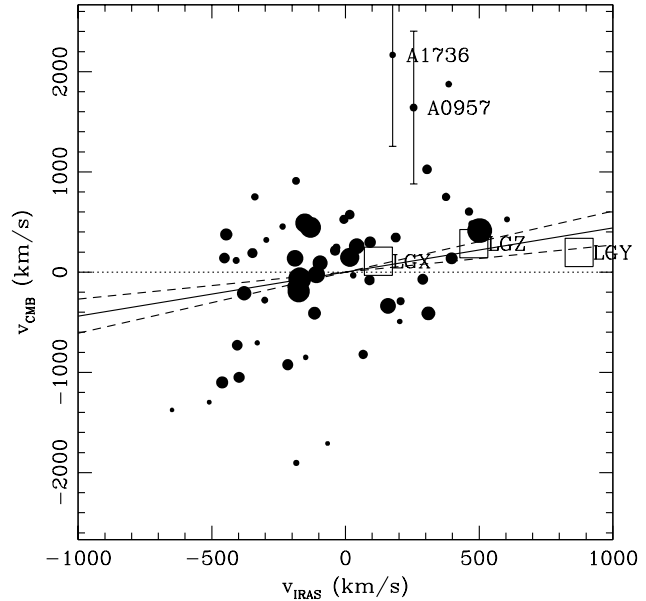


Figure 7. A comparison of observed peculiar velocities and predictions from the PSCz density field with $\beta_{\text{I}} = 1$. SMAC clusters are indicated by filled circles. Clusters which deviate by more than 2σ from the model predictions have error bars plotted and are labelled. Vectorial components of the LG’s peculiar velocity are indicated by open squares and are labelled. The best fitting external bulk flow \mathbf{V}_{ext} has been subtracted from the observations. Symbol sizes scales inversely with observational error. The solid line shows the β_{I} of best fit; dashed lines indicate the errors.

127 km s^{-1} towards $l = 273^\circ \pm 17^\circ$, $b = 6^\circ \pm 15^\circ$. Fig. 7 shows u_{lin} (with $\beta_{\text{I}} = 1$) vs. u_{obs} . The slope of the line of best fit then gives β_{I} .

For our best fit, $\chi^2 = 57.5$ for 54 degrees of freedom. In comparison, the null case of $\beta_{\text{I}} = 0$, $\mathbf{V}_{\text{ext}} = 0$ has $\chi^2 = 95.1$ for 58 degrees of freedom. The marginalized errors quoted above are large because there is strong correlation between the β_{I} and \mathbf{V}_{ext} terms: as β_{I} increases, $|\mathbf{V}_{\text{ext}}|$ drops. The error contours associated with this fit are shown in Fig. 8. The covariance complicates the interpretation of these results. Of the two components of the flow model, β_{I} is the more significant. If \mathbf{V}_{ext} is set to zero, $\beta_{\text{I}} = 0.70 \pm 0.13$, a $> 5\sigma$ detection of β . This “high- β ” model is disfavoured at the 98% CL compared to the model with β_{I} and \mathbf{V}_{ext} free, for which χ^2 falls by 10 with the removal of 3 degrees of freedom. Finally, if β_{I} is fixed at 0.5 (as external comparisons suggest, see below), then we find $\mathbf{V}_{\text{ext}} = 327 \pm 104 \text{ km s}^{-1}$.

It is well known that *IRAS* misses early-type galaxies in the cores of clusters. This effect may be particularly dramatic in regions such as the Shapley Concentration. We have fit a flow model with an attractor at the position of Shapley (core radius 3000 km s^{-1}) in addition to the *IRAS* predictions and an external bulk flow \mathbf{V}_{ext} . For this fit, we find an infall of $129 \pm 84 \text{ km s}^{-1}$ at the LG. This is only $\sim 10 \text{ km s}^{-1}$ less than the infall into SC found above (without the PSCz flow model), indicating that SC is very weak in the PSCz. For this fit the external bulk flow reduces to $300 \pm 140 \text{ km s}^{-1}$.

Table 1. Fits using the PSCz predicted peculiar velocity field

Fit	β_1	$ \mathbf{V}_{\text{ext}} $	l	b	$P(\mathbf{V}_{\text{ext}} = 0)$	χ^2	DOF
With LG	0.39 ± 0.17	372 ± 127	273	6			
With LG	$\equiv 0$	$\equiv 0$				95.1	58
With LG	$\equiv 0$	541 ± 104	269	11	4×10^{-7}	62.7	55
With LG	0.70 ± 0.13	$\equiv 0$				67.3	57
With LG	$\equiv 0.5$	327 ± 104	276	4	8×10^{-3}	57.9	55
No LG	0.87 ± 0.31	637 ± 184	263	-12	1×10^{-3}	53.0	51
No LG	$\equiv 0$	$\equiv 0$				80.4	55
No LG	$\equiv 0$	661 ± 182	261	-2	2×10^{-4}	61.0	52
No LG	0.99 ± 0.28	$\equiv 0$				68.7	54

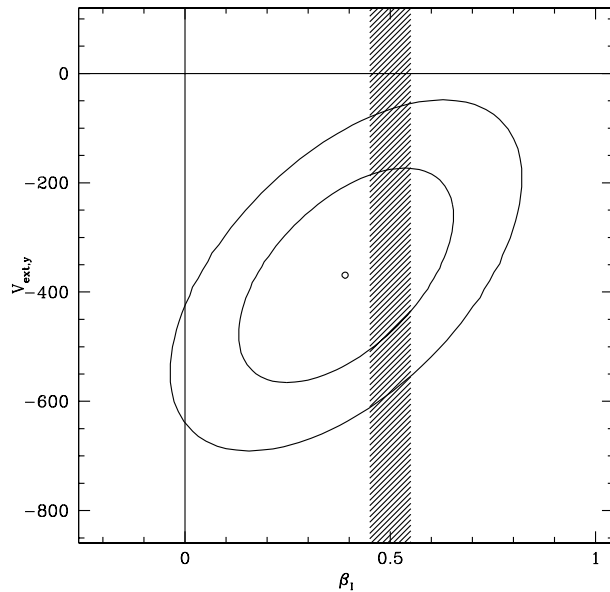


Figure 8. Parameter fits to the SMAC+LG peculiar velocity data using the PSCz predictions. Contours show the 68% and 95% confidence contours on β_1 and the y -component of \mathbf{V}_{ext} . The open circle shows the best fit values. The hashed vertical bar indicates the concordance value of β_1 discussed in Section 5.4.1.

5.4 Discussion

The degeneracy between β and \mathbf{V}_{ext} make it difficult to build a unique flow model from SMAC+LG data alone. There are several independent methods of determining β_1 and \mathbf{V}_{ext} .

5.4.1 External constraints on β_1

(i) **Matching the dipole to the LG’s motion.** This method consists of using equation (6) to predict $\mathbf{v}(0)$ and adjusting β_1 to obtain the best fit with the observed 627 km s^{-1} motion of the LG. If the flow model allows for \mathbf{V}_{ext} as well, then the two components are degenerate (one is fitting 3 data with 4 free parameters). As a result for this method to yield constraints on β_1 one has to make some assumptions for \mathbf{V}_{ext} .

One approach is to allow cosmological models to predict the coherence between a distance-limited gravity dipole and the peculiar velocity of the LG. The most recent estimate of β_1 by this method (Ciecielag & Chodorowski 2004) yields $\beta_1 = 0.64^{+0.24}_{-0.11}$.

(ii) **Fitting peculiar velocity data.** Willick & Strauss (1998) found $\beta_1 = 0.50 \pm 0.04$ by comparing the predictions of the IRAS 1.2 Jy survey to the Mark III data (Willick et al. 1997). Branchini et al. (1999) found $\beta_1 = 0.42 \pm 0.04$ from the comparison of the PSCz to the SFI catalogue Giovanelli et al. (1998). Blakeslee et al. (1999) obtained $\beta_1 = 0.42^{+0.10}_{-0.06}$ from a comparison of Surface Brightness Fluctuation survey peculiar velocities to IRAS 1.2 Jy predictions. These three analyses are conducted in the LG frame and are insensitive to \mathbf{V}_{ext} . Zaroubi et al. (2002) found $\beta_1 = 0.51 \pm 0.06$ from comparison of ENEAR (da Costa et al. 2000b) and SFI peculiar velocities to PSCz in the CMB frame.

(iii) **Redshift-space distortions.** Hamilton et al. (2000) found $\beta_1 = 0.41^{+0.13}_{-0.12}$ from an analysis of redshift-space distortions in the PSCz survey. Taylor et al. (2001) found essentially identical results.

(iv) **Expectations from cosmological models.** Using the WMAP, 2dF and Lyman- α forest data, Spergel et al. (2003) found $\Omega_m^{0.6} \sigma_8 = 0.38^{+0.04}_{-0.05}$. Combining this with the measurement $\sigma_{8,1} = 0.80 \pm 0.05$ from Hamilton & Tegmark (2002), we obtain $\beta_1 = 0.48 \pm 0.06$.

The “concordance” value $\beta_1 = 0.5$ is consistent with all of the above determinations at the 2σ level. Note that the value $\beta_1 = 0.5$ requires a residual motion of $\sim 160 \text{ km s}^{-1}$ towards $l = 319^\circ$, $b = 13^\circ$ (or $V_x = 119$, $V_y = -110$, $V_z = 35$) from outside the PSCz volume (i.e. from beyond $200 h^{-1} \text{ Mpc}$ or in the Zone of Avoidance) in order to match the observed peculiar velocity of the LG.

5.4.2 External constraints on \mathbf{V}_{ext}

What is the expected value of \mathbf{V}_{ext} ? There are four sources of uncertainty in the PSCz predicted peculiar velocities.

(i) **Shot noise within $R \sim 200h^{-1} \text{ Mpc}$.** At $R = 150h^{-1} \text{ Mpc}$, Schmoltd et al. (1999) quote errors of $160\beta_1 \text{ km s}^{-1}$ on the predicted velocity of the LG. They do not extend their analysis to greater distances, but an eyeball extrapolation of their Figure 5 suggests that this grows to $\sim 200\beta_1$ at $R = 200h^{-1} \text{ Mpc}$.

(ii) **Sources in the Galactic Plane.** Saunders et al. (2000a) published preliminary results from the “Behind the Plane” (BTP) survey (an extension of the PSCz to lower Galactic latitudes). The BTP dipole in units of km s^{-1} (assuming $\beta_1 = 0.5$), grows from $V_x = -60$, $V_y = -325$, $V_z = 350$ at $R \sim 100h^{-1} \text{ Mpc}$, to $V_x = -60$, $V_y = -475$, $V_z = 350$ at $R \sim 200h^{-1} \text{ Mpc}$. The misalignment with the CMB dipole of only $\sim 13^\circ$. At $R \sim 300h^{-1} \text{ Mpc}$, the dipole is $V_x = -25$, $V_y = -675$, $V_z = 350$, or $\sim 761 \text{ km s}^{-1}$ towards $l = 268^\circ$, $b = 27^\circ$, and the misalignment is reduced to $\sim 8^\circ$. The BTP dipole is in better directional agreement with the

LG’s observed motion than the PSCz dipole. It is possible that this alignment is fortuitous since the shot-noise effects (and systematics such as the “rocket-effect” (Kaiser 1987)) are likely to be large beyond $200 h^{-1}\text{Mpc}$. There is a particularly strong change in V_y in the range $180\text{--}240 h^{-1}\text{Mpc}$ which is present in both the PSCz and BTP dipoles, but is much stronger in the latter. This suggests that there are dynamically important structures close to the Galactic Plane.

For purposes of assessing V_{ext} result from the SMAC sample, an estimate of the effect of hidden sources in the Plane is given by the difference between the growth in the BTP dipole and the PSCz dipole at distances beyond the SMAC sample ($\sim 100 h^{-1}\text{Mpc}$). The difference in km s^{-1} for $\beta_1 = 0.5$ is $\Delta V_x = +105$, $\Delta V_y = -135$, $\Delta V_z = -20$, or 172 km s^{-1} towards $l = 308^\circ$, $b = -7^\circ$. We estimate the error on this to be 50% or 85 km s^{-1} .

The “Clusters Behind the Zone of Avoidance” (CIZA), an X-ray selected survey galaxy clusters, Ebeling et al. (2002) also indicates several massive clusters at low galactic latitudes. However, these appear to be located either in the vicinity of the GA at $60 h^{-1}\text{Mpc}$ (A3627 and CIZAJ1324.7-5736) or nearer to SC at a distance of $\sim 150 h^{-1}\text{Mpc}$ (CIZA J1653.0-5943 and Triangulum Australis) and not at $180\text{--}240 h^{-1}\text{Mpc}$ suggested by the BTP dipole. The gravity dipole of the CIZA sample (Kocevski et al. 2003) has a strong contribution at $150 h^{-1}\text{Mpc}$ which is not seen in the PSCz or the BTP.

(iii) **Sources beyond $200 h^{-1}\text{Mpc}$.** Since the PSCz/BTP data are noisy beyond $200 h^{-1}\text{Mpc}$, it is difficult to assess this empirically. For a ΛCDM cosmological model with $\Gamma = 0.21$, $\Omega_m = 0.3$, $n = 1$ and $\sigma_8 = 1$, we expect the rms contribution to the bulk motion in the nearby Universe arising from sources beyond $200 h^{-1}\text{Mpc}$ to be $\sim 50 \text{ km s}^{-1}$ in each component.

(iv) **Missing contributions from high-density superclusters.** *IRAS* does not detect early-type galaxies. For individual clusters this is a weak effect, which can be compensated by increasing β_1 . There are certain extreme regions, such as the SC and the Horologium-Reticulum superclusters, where there is an astounding excess of clusters. For example, Tully et al. (1992) find 29 Abell/ACO clusters within $50 h^{-1}\text{Mpc}$ of the centre of the SC. This corresponds to a mean overdensity $\delta_c \sim 5$ in clusters. If $b_c/b_1 \sim 4$, (Branchini et al. 1999), then we expect the PSCz overdensity to be $\delta_l \sim 1.25$, yielding an infall at the LG of $250\beta_1 \text{ km s}^{-1}$. In fact, the observed PSCz overdensity is only 0.2, yielding an infall of only $40\beta_1 \text{ km s}^{-1}$. A similar situation occurs for the Horologium-Reticulum supercluster. Tully et al. finds a cluster overdensity of ~ 4 on scales of $50 h^{-1}\text{Mpc}$ but the PSCz overdensity is only 0.14. Clearly linear biasing does not operate in these very high-density regimes.

Because the cluster overdensity is likely an overestimate of the true mass density (even when scaled by $b_1/b_c \sim 0.25$), and the PSCz overdensity an underestimate, one might expect the true situation to lie in between. For $\beta_1 = 0.5$, we will estimate a residual dipole of $\sim 50 \pm 25 \text{ km s}^{-1}$ in the direction of the SC, and, because it is at greater distance, half of that for Horologium-Reticulum.

Adding the BTP residual dipole (172 km s^{-1} toward $l = 308^\circ$, $b = -7^\circ$), plus contributions directed to SC (50 km s^{-1}) and HR (25 km s^{-1}), we obtain an estimate of $V_{\text{ext}} = 225 \text{ km s}^{-1}$ towards $l = 305^\circ$, $b = -4^\circ$. Most of this is due to the extra Galactic Plane sources in the BTP dipole. Errors on V_{ext} estimated to be 90 km s^{-1} (systematic uncertainty) and 75 (shot noise) and 50 (residual beyond $200 h^{-1}\text{Mpc}$). Summed in quadrature, this yields an error of 150 km s^{-1} . Clearly, given the uncertainties,

there is no firm external evidence that V_{ext} is required. The fact that the best estimate is an agreement with the measured direction and amplitude of V_{ext} from the SMAC survey ($372 \pm 127 \text{ km s}^{-1}$ towards $l = 273^\circ \pm 17^\circ$, $b = 6^\circ \pm 15^\circ$) suggests that these external sources do exist.

6 COMPARISON WITH OTHER RESULTS

The bulk flow calculated in this paper is a statistic derived from the SMAC sample. This is not to suggest that the true flow field within 12000 km s^{-1} is a pure dipole bulk flow. Indeed, a pure dipole velocity field is unlikely given that the mass density field is a Gaussian random field with fluctuation power on a range of scales. Due to sparse sampling, the bulk flow of any peculiar velocity sample will have contributions from the true bulk flow of the volume, as well as from higher order multipoles. This effect was first emphasized by Watkins & Feldman (1995). It would, therefore, be naive to compare the bulk flow from different sparsely-sampled surveys without allowing for the error introduced by sparse sampling. Nevertheless, that has been the approach taken in the past, and it has led to an exaggeration of the differences between various studies.

A full statistical comparison between surveys, based on the three components of the bulk flow and the full error covariance matrices allowing for the above-mentioned sparse sampling effects, is beyond the scope of the present paper. A preliminary comparison of the bulk flows of SMAC, Willick (1999), LP, Dale et al. (1999), Colless et al. (2001, hereafter EFAR), and the SNIa compilation of Tonry et al. (2003) has been performed by Hudson (2003), who concluded that there was no inconsistency between any of these surveys, except possibly for LP which is inconsistent at the 94% level.

Instead of the full vectorial comparison, in this paper we opt for a simpler, illustrative comparison which considers simply the component of the bulk flow projected along a given axis directed towards $l = 300^\circ$, $b = 10^\circ$. This “concordance” direction has been chosen because it is close to the mean flow of the above-mentioned sparse surveys (Hudson 2003), is within a few degrees of the Supergalactic Plane, and is also very close to the bulk motion originally reported for the 7S sample by Dressler et al. (1987). In his analysis of the Mark II peculiar velocity catalogue, Hudson (1994) found that the gravity of the local density field to 8000 km s^{-1} could not account for a residual bulk motion of $400 \pm 45 \text{ km s}^{-1}$ toward $l = 292^\circ$, $b = 7^\circ$. If this model is correct, then deeper surveys such as SMAC should have bulk flows close to this residual motion.

For the SMAC sample, with the bulk flow fixed in the concordance direction $l = 300^\circ$, $b = 10^\circ$, the best fitting amplitude is $400 \pm 120 \text{ km s}^{-1}$. The following sections compare our results with those from other surveys, focussing first on those based on sparse samples on large scales.

6.1 Large-scale Surveys

6.1.1 Brightest Cluster Galaxies

Lauer & Postman (1994) found a bulk flow of $689 \pm 178 \text{ km s}^{-1}$ towards $l = 343^\circ$, $b = +52^\circ$ from 119 clusters using the distance indicator based on the photometry of brightest cluster galaxies (BCGs). The direction of the SMAC bulk flow is nearly 90° away from that of LP, so these two results appear to be in poor agreement. Nor does LP agree with results from other peculiar velocity surveys (Dale et al. 1999, EFAR). The LP sample is denser

than other all-sky surveys on similar scales and so it is less affected by sampling errors than other sparser surveys, including SMAC. Therefore sparse sampling is unlikely to be a source of disagreement between LP and other surveys.

In SMAC-IV, we compared our cluster distances with those of LP. We found that of 41 clusters in common, four were discrepant at greater than the 2σ level: A262, A1060 (Hydra), A3381 and A3733. In all cases, comparison with the observed redshifts indicates that the LP distances are too long corresponding to BCG magnitudes which are too faint.

One possible explanation for this discrepancy is obscuration by dust in BCGs. Laine et al. (2003) examined dust in 75 of LP's 119 BCGs. They found signs of dust in $\sim 38\%$ of BCGs. In some cases the dust appears to be quite extended, and this could affect the LP magnitudes.

There is evidence that galaxies classified by Laine et al. as having filamentary or patchy dust are systematically too faint. If we compare the ratios of the estimated distance from the LP BCG method to the distance estimated by assuming that the BCG is at rest with respect to the CMB, we find that for 49 galaxies with no dust the distance ratio is 0.98 ± 0.02 . Galaxies with only nuclear ($\lesssim 1''$) dust disks (Laine code “D”), dust spirals (code “S”), or rings (code “R”) have a distance ratio 0.92 ± 0.04 . These small scale features are unlikely to affect the $10 h^{-1}\text{kpc}$ aperture magnitude which corresponds to a much larger angular scale, typically tens of arcseconds (Postman & Lauer 1995). However, the distance ratios are higher for galaxies with filamentary (“F”) dust (1.06 ± 0.06), patchy (“P”) dust (1.12 ± 0.08) or both patchy and filamentary dust (1.28 ± 0.10). The latter category consists of only 4 galaxies, the BCGs of A0262, A1060, A3698 and A3733. Three of these (A0262, A1060 and A3733) clearly have very extended dust in gray scale images (fig. 1 of Laine et al.). These same three galaxies are extreme outliers in the SMAC vs. LP comparison discussed above.

If we remove from LP's sample the 19 galaxies with dust classified as filamentary or patchy (or both) in Laine et al.'s Table 2, we obtain a bulk flow of $707 \pm 261 \text{ km s}^{-1}$ toward $l = 336^\circ \pm 46^\circ$, $b = 38^\circ \pm 23^\circ$. The error-bias-corrected amplitude is 384 km s^{-1} (to be compared with LP's quoted 689 km s^{-1}). A3381 is not in the Laine et al. sample, but is the most discrepant cluster in the SMAC-LP distance comparison performed in Paper IV (3.7σ). While this cluster has a somewhat larger internal FP scatter (Jorgensen et al. 1996), its SMAC peculiar velocity is not significant $1103 \pm 679 \text{ km s}^{-1}$. In contrast, its peculiar velocity according to LP is large and significantly different from zero ($-5900 \pm 2100 \text{ km s}^{-1}$), so we suspect that for this object LP are in error, rather than SMAC. If we also remove A3381, the LP bulk motion becomes $667 \pm 242 \text{ km s}^{-1}$ towards $l = 315^\circ \pm 48^\circ$, $b = 35^\circ \pm 26^\circ$. This differs from no bulk flow, but only at a marginal (95%) confidence level. This is in better agreement (both in direction and amplitude) with the SMAC bulk flow. Along the direction $l = 300^\circ$, $b = 10^\circ$, the motion of this sample is $700 \pm 380 \text{ km s}^{-1}$. Note that because of the error ellipsoid is triaxial it is possible that a flow solution fixed along a given direction has a higher amplitude than that of the flow along the direction of best fit.

There is therefore a strong hint that the original LP sample was affected by dust. Although it is tempting to use the result from the culled sample as a “corrected” LP bulk flow, it is important to remember that there remain 25 galaxies in the BCG sample of LP which are neither in Laine et al. sample nor have comparison peculiar velocity data from SMAC. It is likely that some ($\sim 25\%$) of these will be strongly affected by dust. Furthermore, it is also possi-

ble that the LP motion is affected by other systematics, such as the tendency for brighter BCGs to inhabit more X-ray-luminous clusters (Hudson & Ebeling 1997). We conclude that the original LP result is in marginal disagreement with SMAC, but this disagreement is no longer significant once some BCGs with clear evidence of dust are removed from the LP sample.

6.1.2 Tully-Fisher distances to clusters

Mould et al. (1993) observed 38 TF clusters and fitted a bulk flow of $811 \pm 138 \text{ km s}^{-1}$ towards $l = 332^\circ$, $b = -15^\circ$. Along the “concordance” direction, this projects to $617 \pm 138 \text{ km s}^{-1}$. Excluding two outliers (NGC 5419 and A3627), they obtained a flow of $559 \pm 107 \text{ km s}^{-1}$ toward $l = 326^\circ$, $b = -9^\circ$ or $473 \pm 107 \text{ km s}^{-1}$ toward $l = 300^\circ$, $b = 10^\circ$.

Willick (1999) found a bulk flow of $961 \pm 280 \text{ km s}^{-1}$ toward $l = 266^\circ$, $b = 19^\circ$ from 15 clusters using the Tully-Fisher relation. The amplitude and direction are in excellent agreement with SMAC bulk flow, although the errors are large. Along the “concordance” direction, the flow of the Willick (1999) sample is $820 \pm 410 \text{ km s}^{-1}$.

In contrast, Dale et al. (1999) found a bulk flow of only $75 \pm 92 \text{ km s}^{-1}$ towards $l = 289^\circ$, $b = 25^\circ$ (with large errors in the direction due to the small amplitude of the bulk flow) from TF distances in 64 clusters with a similar depth as the SMAC sample (but with different spatial sampling). The amplitude is consistent with zero. If we fix the direction to be $l = 300^\circ$, $b = 10^\circ$, our fits yield an amplitude of $120 \pm 120 \text{ km s}^{-1}$. This is consistent with the SMAC flow in this direction.

6.1.3 EFAR

Colless et al. (2001) studied 50 clusters in two distinct regions of the sky (Perseus-Pisces and Hercules-Corona-Borealis) via the FP method. They found no significant bulk flow for the EFAR sample.

The geometry of the EFAR survey introduces several subtle problems. First, there is substantial covariance between the monopole (FP zero-point) and dipole terms, with a correlation coefficient of -0.77 between the monopole term and the Galactic y -component of the EFAR bulk flow. Since the SMAC bulk flow is essentially along the y direction, this is clearly an important issue. Colless et al. fixed the zero-point of the EFAR FP relation by assuming that a subset of their clusters were at rest. However, for an anisotropic sample such as EFAR, this choice presupposes that there is no bulk flow. They studied the effect of this choice and concluded that it was smaller than their random errors. While this is correct, it is not negligible and should be included in the total errors. Second, irrespective of the monopole covariance, the effects of sampling are particularly severe for the EFAR sample, which covers two specific regions on the sky.

We have fit the EFAR peculiar velocities to flow models including both a bulk flow and free zero-point. Note that, because we are fitting a flow model to distances a posteriori (Method I of Strauss & Willick 1995), we apply homogeneous Malmquist bias corrections to the EFAR cluster distances. We also allow for distance errors due to errors in the extinctions, in the same way as for the SMAC data. Note, however, that the EFAR errors used in this analysis do not include the unpublished systematic errors due to matching the velocity dispersion systems. We expect these to be at a level at least that found for the SMAC sample.

A fit of the EFAR data yields a bulk flow of $629 \pm 381 \text{ km s}^{-1}$

towards $l = 53^\circ \pm 41^\circ$, $b = 6^\circ \pm 25^\circ$. If we force EFAR to have the same bulk flow as the SMAC sample, we find $\Delta\chi^2 = 11$ for an increase of three degrees of freedom. Thus the *best fit* value of the SMAC bulk flow is rejected at the 98.9% CL. This does not mean that EFAR results are inconsistent with the SMAC results. In the direction $l = 300^\circ$, $b = 10^\circ$, the EFAR amplitude is $120 \pm 310 \text{ km s}^{-1}$, which is consistent with the SMAC value $400 \pm 120 \text{ km s}^{-1}$.

6.1.4 SNIa

We have analyzed 98 SNe within $150 h^{-1}\text{Mpc}$ from the compilation of Tonry et al. (2003). Details of this analysis will be presented elsewhere. In summary, we find that the sample as a whole has a bulk flow of $410 \pm 75 \text{ km s}^{-1}$ towards $l = 286^\circ$, $b = -12^\circ$. However the effective depth of this sample is only $35h^{-1} \text{ Mpc}$. To test the coherence of the flow, we have split the sample into two subsamples: SNIa-In ($0 < r < 60h^{-1} \text{ Mpc}$) and SNIa-Out ($60 < r < 150h^{-1} \text{ Mpc}$). The SNIa-In sample has a bulk flow of $376 \pm 81 \text{ km s}^{-1}$ toward $l = 285^\circ$, $b = -14^\circ$, which is not surprising since this subsample spans a distance range where flows are known to be high. The SNIa-Out sample has a bulk flow of $775 \pm 204 \text{ km s}^{-1}$ toward $l = 299^\circ \pm 17^\circ$, $b = 3^\circ \pm 13^\circ$. The bulk flow of the outer sample is significantly different from zero at the 99.8% CL. The direction and amplitude of the SNIa-Out subsample are in good agreement with the SMAC bulk flow.

6.1.5 Comparison of large-scale surveys

Fig. 9 compares the error-ellipsoids in the V_x - V_y plane for the SMAC, SNIa-Out and Dale et al samples. Note that these errors are due to peculiar velocity errors only. They do not include the effects of sparse sampling which would tend to further increase the errors. These three surveys are the ones which, with the exception of LP, are most discrepant given their bulk flows and errors. Despite these differences there is a ‘‘concordance’’ region in which the flow is $250\text{--}450 \text{ km s}^{-1}$. The bulk flows of other surveys mentioned in this section cover this concordance region and do not further constrain it.

6.2 Field surveys within approximately $60h^{-1} \text{ Mpc}$

The peculiar velocity field has also been mapped at higher density within smaller volumes closer to the LG. For these samples, it is possible to obtain a bulk flow which is less contaminated by sampling effects.

(i) Giovanelli et al. (1998) studied a large sample of TF field galaxies. They found a bulk flow of $200 \pm 65 \text{ km s}^{-1}$ towards $l = 295^\circ$, $b = 25^\circ$ for the volume extending to 6500 km s^{-1} .

(ii) Within $50 h^{-1}\text{Mpc}$, the bulk flow of the Mark III sample (Willick et al. 1997) is $305 \pm 110 \text{ km s}^{-1}$ toward $l = 313^\circ$, $b = 29^\circ$ when volume-weighted (Dekel et al. 1999) via the POTENT method. The corresponding result for the SFI survey is $310 \pm 80 \text{ km s}^{-1}$ toward $l = 299^\circ$, $b = 29^\circ$. Dekel et al. (1999) argue that this flow is generated from beyond $50 h^{-1}\text{Mpc}$.

(iii) The Shellflow project (Courteau et al. 2000) studied TF galaxies in the range $4500 < cz < 7000 \text{ km s}^{-1}$ and found $V = 70_{-70}^{+100} \text{ km s}^{-1}$, with a 95% upper limit of $V < 300 \text{ km s}^{-1}$. Due to the small amplitude of the flow in comparison with the errors, the direction is not well defined: $l = 144^\circ \pm 140^\circ$, $b = 50^\circ \pm 79^\circ$.

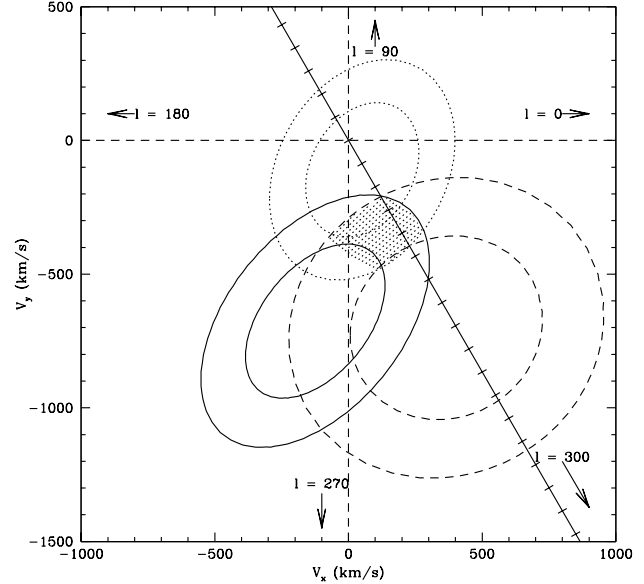


Figure 9. Galactic x and y components of the bulk flow and their 68% and 95% confidence level error ellipsoids. We have plotted results for the large-scale sparse surveys SMAC (solid), Dale et al. (dotted) and SNIa with $60h^{-1} \text{ Mpc} < d < 150h^{-1} \text{ Mpc}$ (dashed). These surveys all have very small components in the z direction. Solutions that lie within the 95% confidence region of all three surveys are hatched. These three samples which differ the most in their flows and hence set the tightest bounds on the concordance region. The concordance direction $l = 300^\circ$, $b = 10^\circ$ is indicated by the solid diagonal line. The EFAR and Willick results are not plotted as their errors are considerably larger. The results of Mould et al. are not plotted here but are also consistent with this concordance region. In contrast to the other surveys, the LP bulk flow vector does have a large z component and so its motion is not well-represented by plotting ellipses in the x - y plane.

(iv) The ENEAR sample of early-type galaxies within $cz < 7000 \text{ km s}^{-1}$ has a bulk flow of $V = 220 \pm 60$ (random) ± 50 (systematic) km s^{-1} toward $l = 304^\circ \pm 16^\circ$, $b = 25^\circ \pm 11^\circ$ (da Costa et al. 2000).

(v) Tonry et al. (2000) did not measure a bulk flow of their SBF sample. Instead, they fitted a combination of internal flows (from GA and Virgo) plus external dipole and quadrupole terms. The external dipole is $\sim 150 \text{ km s}^{-1}$ toward $l = 294^\circ$, $b = 67^\circ$. The errors on this amplitude are difficult to estimate because of the large degeneracies with the GA infall, but are approximately 100 km s^{-1} .

In summary, with the exception of Shellflow, the field surveys find a consistent non-zero flow in a similar direction on the sky. Note, however, that the three TF samples (Mark III, SFI, Shellflow) are not independent. A conservative estimate of the bulk flow within $60 h^{-1}\text{Mpc}$ from field TF and FP data is $\sim 200 \pm 75 \text{ km s}^{-1}$.

6.3 Towards a consistent model for large-scale flows

The bulk flows of all surveys discussed above, projected into the direction $l = 300^\circ$, $b = 10^\circ$ are shown in Fig. 10. Surveys are plotted as a function of their estimated depth. The lines indicate IRAS PSCz predictions for the bulk flow along this direction for different values of β_1 and V_{ext} . An eyeball fit reveals that $V_{\text{ext}} = 0$ is excluded by

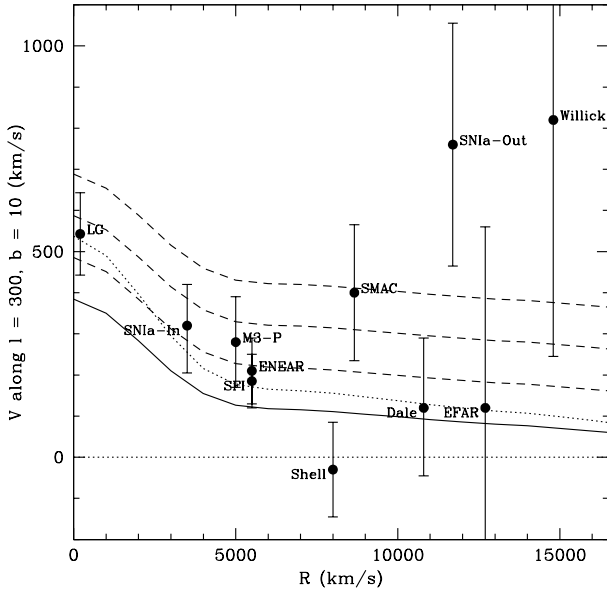


Figure 10. The bulk flow projected along the direction $l = 300^\circ$, $b = 10^\circ$ as a function of depth, for the LG and various surveys: SNIa with $r < 60h^{-1}$ Mpc (SNIa-In), Dekel et al. (1999) analysis of the Mark III sample (M3-P), SFI, ENEAR, Shellflow, SMAC, distant ($60h^{-1}$ Mpc $< r < 150h^{-1}$ Mpc) SNe (SNIa-out), EFAR and Willick (1999). Error bars are 1σ and do not include the effects of sparse sampling. Surveys are placed approximately at the depth corresponding to the top-hat radius of an idealized volume-weighted survey with the same effective depth. This estimate is very crude: horizontal error bars on the depth are $\sim 10h^{-1}$ Mpc for the nearby samples and $\sim 20h^{-1}$ Mpc for the distant ones. The solid curve shows the bulk flow predicted from the PSCz survey if $\beta_I = 0.5$, whereas the dotted line shows the predicted bulk flow for $\beta_I = 0.7$. The dashed lines show the PSCz bulk flow with V_{ext} of 100, 200 and 300 km s^{-1} .

the distant samples, in particular SMAC and the SNIa-Out sample. Similarly, a bulk flow with $V = 600 \text{ km s}^{-1}$ is also excluded, in particular by Dale et al. (1999) and Shellflow.

A reasonable fit to all samples is possible if $\beta_I = 0.5$, producing a bulk flow component of $\sim 100 \text{ km s}^{-1}$ in this direction at $R = 100h^{-1}$ Mpc from sources in the PSCz survey, plus an additional V_{ext} component from sources not included in PSCz. Most of the field peculiar surveys are consistent V_{ext} of approximately 125 km s^{-1} , with the exception of Shellflow which prefers $V_{\text{ext}} \sim 0$. The deeper surveys prefer a higher value $V_{\text{ext}} \sim 200 \text{ km s}^{-1}$. It is difficult, however, to quantify the effects of sparse sampling, particularly on the latter surveys. Inspection of Fig. 10 suggests that $V_{\text{ext}} = 125 \text{ km s}^{-1}$ is consistent with almost all of the peculiar velocity surveys. There appear to be two exceptions: Shellflow, which lies too low, and the SNIa-Out sample, which is too high. Since both of these samples have unusual geometry — Shellflow because it is a shell, and the SNIa-Out sample because it is sparse — it is likely that sampling errors will contribute significantly to the error bars.

By adding $V_{\text{ext}} = 125 \text{ km s}^{-1}$ to the 100 km s^{-1} contribution from the PSCz density field, one finds that 225 km s^{-1} , or a third of the LG’s motion arises from sources at large scales ($R > 100h^{-1}$ Mpc). Given the systematic uncertainties and effects of sampling, we estimate the error on this value is approximately 100 km s^{-1} .

7 CONCLUSIONS

We have examined in detail the $687 \pm 203 \text{ km s}^{-1}$ bulk flow of the SMAC sample and find that it is robust to systematic errors. We have shown that most of the bulk flow is not generated by nearby sources such as the Great Attractor but rather arises from structures at depths greater than $100h^{-1}$ Mpc. The Shapley Concentration is identified as one likely source of the large scale flow but is unlikely to be responsible for all of the SMAC flow.

When we compare the SMAC motion to the predictions of the PSCz survey we find that $\beta = 0.39 \pm 0.17$, consistent with the “concordance” value $\beta \sim 0.5$. However, the *IRAS* PSCz survey can only explain $50 \pm 20\%$ of the amplitude of the SMAC flow. This suggests that there are gravitational sources not well-mapped by the PSCz survey. Evidence from other redshift surveys suggests that these sources may be located in the ZOA or in superclusters such as Shapley which are undersampled by *IRAS*.

Finally, we have shown that the SMAC survey is not inconsistent with other sparsely-sampled surveys of the large scale velocity field, such as Dale et al. (1999); Willick (1999, EFAR) and the SNe sample of Tonry et al. (2003). Taken together, all surveys suggest a large scale flow approximately 225 km s^{-1} towards $l = 300^\circ$, $b = 10^\circ$. Further analyses of the effects of sparse sampling, and detailed comparisons with the predictions of redshift surveys such as PSCz are needed to more accurately quantify this result.

The NOAO Fundamental Plane Survey (Smith et al. 2004) will measure the peculiar velocities of 100 X-ray selected clusters. The total number of FP distances will be ~ 4000 , about six times the number in SMAC. When results from the NFPS are compared to, for example, predictions of the 2MASS redshift survey (Huchra et al. 2003), we expect to identify the sources the LG’s motion.

ACKNOWLEDGMENTS

The data used in this project were obtained at the Isaac Newton Group of telescopes at the Observatorio del Roque de los Muchachos, the Anglo- Australian Observatory, and the Cerro Tololo Inter-American Observatory. MJH acknowledges financial support from the NSERC and a Premier’s Research Excellence Award.

REFERENCES

- Blakeslee J.P., Davis M., Tonry J.L., Dressler A., Ajhar E.A., 1999, *ApJ*, 527, L73
- Blakeslee J.P., Lucey J.R., Barris B.J., Hudson M.J., Tonry J.L., 2001, *MNRAS*, 327, 1004
- Blakeslee J.P., Lucey J.R., Tonry J.L., Hudson M.J., Narayanan V.K., Barris B.J., 2002, *MNRAS*, 330, 443
- Branchini E., et al., 1999, *MNRAS*, 308, 1
- Burstein D., Heiles C., 1982, *AJ*, 87, 1165 (BH)
- Ciecielag P., Chodorowski M., 2004, *astro-ph/0401195*
- Colless M., Saglia R.P., Burstein D., Davies R.L., McMahan R.K., Wegner G., 2001, *MNRAS*, 321, 277 (EFAR)
- Courteau S., 1992, *PASP*, 104, 976
- Courteau S., Dekel A., 2001, in von Hippel T., Simpson C., Manset N., eds., *Astrophysical Ages and Time Scales*, *Astronomical Society of the Pacific*
- Courteau S., Willick J.A., Strauss M.A., Schlegel D., Postman M., 2000, *ApJ*, 544, 636

- da Costa L.N., Bernardi M., Alonso M.V., Wegner G., Willmer C.N.A., Pellegrini P.S., Maia M.A.G., Zaroubi S., 2000, *ApJ*, 537, L81
- da Costa L.N., Bernardi M., Alonso M.V., Wegner G., Willmer C.N.A., Pellegrini P.S., Rit e C., Maia M.A.G., 2000b, *AJ*, 120, 95 (ENEAR)
- Dale D.A., Giovanelli R., Haynes M.P., Campusano L.E., Hardy E., Borgani S., 1999, *ApJ*, 510, L11
- Dekel A., Eldar A., Kolatt T., Yahil A., Willick J.A., Faber S.M., Courteau S., Burstein D., 1999, *ApJ*, 522, 1
- Dressler A., 1988, *ApJ*, 329, 519
- Dressler A., Faber S.M., Burstein D., Davies R.L., Lynden-Bell D., Terlevich R.J., Wegner G., 1987, *ApJ*, 313, L37
- Ebeling H., Mullis C.R., Tully R.B., 2002, *ApJ*, 580, 774
- Faber S.M., Wegner G., Burstein D., Davies R.L., Dressler A., Lynden-Bell D., Terlevich R.J., 1989, *ApJS*, 69, 763
- Gibbons R.A., Fruchter A.S., Bothun G.D., 2001, *AJ*, 121, 649
- Giovanelli R., Dale D.A., Haynes M.P., Hardy E., Campusano L.E., 1999, *ApJ*, 525, 25
- Giovanelli R., Haynes M.P., Freudling W., da Costa L.N., Salzer J.J., Wegner G., 1998, *ApJ*, 505, L91 (SFI)
- Hamilton A.J.S., Tegmark M., 2002, *MNRAS*, 330, 506
- Hamilton A.J.S., Tegmark M., Padmanabhan N., 2000, *MNRAS*, 317, L23
- Huchra J., Jarrett T., Skrustkie M., Cutri R., Schneider S., Macri L., Steining R., Mader J., 2003, in *IAU Symposium*
- Hudson M.J., 1993, *MNRAS*, 265, 43
- Hudson M.J., 1994, *MNRAS*, 266, 475
- Hudson M.J., 1999, *PASP*, 111, 57
- Hudson M.J., 2003, in Bartlett J., ed., *Proceedings of the 15th Rencontres De Blois: Physical Cosmology: New Results In Cosmology And The Coherence Of The Standard Model*, in press (astro-ph preprint 0311072)
- Hudson M.J., Ebeling H., 1997, *ApJ*, 479, 621
- Hudson M.J., Lucey J.R., Smith R.J., Schlegel D.J., Davies R.L., 2001, *MNRAS*, 327, 265 (SMAC-III)
- Hudson M.J., Lucey J.R., Smith R.J., Steel J., 1997, *MNRAS*, 291, 488 (PP-II)
- Hudson M.J., Smith R.J., Lucey J.R., Schlegel D.J., Davies R.L., 1999, *ApJ*, 512, L79
- Jorgensen I., Franx M., Kjaergaard P., 1996, *MNRAS*, 280, 167
- Kaiser N., 1987, *MNRAS*, 227, 1
- Kocevski D.D., Ebeling H., Mullis C.R., 2003, astro-ph/0304453
- Kogut A., et al., 1993, *ApJ*, 419, 1
- Kolatt T., Dekel A., Lahav O., 1995, *MNRAS*, 275, 797
- Kraan-Korteweg R.C., Woudt P.A., Cayatte V., Fairall A.P., Balkowski C., Henning P.A., 1996, *Nature*, 379, 519
- Laine S., van der Marel R.P., Lauer T.R., Postman M., O'Dea C.P., Owen F.N., 2003, *AJ*, 125, 478
- Lauer T.R., Postman M., 1994, *ApJ*, 425, 418 (LP)
- Lilje P.B., Yahil A., Jones B.J.T., 1986, *ApJ*, 307, 91
- Lynden-Bell D., Faber S.M., Burstein D., Davies R.L., Dressler A., Terlevich R.J., Wegner G., 1988, *ApJ*, 326, 19
- Mathewson D.S., Ford V.L., Buchhorn M., 1992, *ApJ*, 389, L5
- Mould J.R., Akeson R.L., Bothun G.D., Han M., Huchra J.P., Roth J., Schommer R.A., 1993, *ApJ*, 409, 14
- Ostriker J.P., Suto Y., 1990, *ApJ*, 348, 378
- Postman M., Lauer T.R., 1995, *ApJ*, 440, 28
- Saunders W., et al., 2000a, in Kraan-Korteweg R.C., Henning P.A., Andernach H., eds., *ASP Conf. Ser. 218: Mapping the Hidden Universe: The Universe behind the Milky Way - The Universe in HI*, *Astronomical Society of the Pacific*, 141
- Saunders W., et al., 2000b, *MNRAS*, 317, 55
- Schlegel D.J., Finkbeiner D.P., Davis M., 1998, *ApJ*, 500, 525 (SFD)
- Schmoldt I., et al., 1999, *MNRAS*, 304, 893
- Smith R.J., Lucey J.R., Hudson M.J., Schlegel D.J., Davies R.L., 2000, *MNRAS*, 313, 469 (SMAC-I)
- Smith R.J., Lucey J.R., Schlegel D.J., Hudson M.J., Baggley G., Davies R.L., 2001, *MNRAS*, 327, 249 (SMAC-II)
- Smith R.J., et al., 2004, submitted to *AJ*
- Smoot G.F., Gorenstein M.V., Muller R.A., 1977, *Physical Review Letters*, 39, 898
- Spergel D.N., et al., 2003, astro-ph/0302209
- Staveley-Smith L., Juraszek S., Koribalski B.S., Henning P.A., Kraan-Korteweg R.C., 2000, astro-ph/0009223
- Strauss M.A., Cen R., Ostriker J.P., Lauer T.R., Postman M., 1995, *ApJ*, 444, 507
- Strauss M.A., Davis M., Yahil A., Huchra J.P., 1992, *ApJ*, 385, 421
- Strauss M.A., Willick J.A., 1995, *Phys. Rep.*, 261, 271
- Taylor A.N., Ballinger W.E., Heavens A.F., Tadros H., 2001, *MNRAS*, 327, 689
- Tonry J.L., Blakeslee J.P., Ajhar E.A., Dressler A., 2000, *ApJ*, 530, 625 (SBF)
- Tonry J.L., et al., 2003, *ApJ*, 594, 1
- Tully R.B., Scaramella R., Vettolani G., Zamorani G., 1992, *ApJ*, 388, 9
- Watkins R., Feldman H.A., 1995, *ApJ*, 453, L73
- Willick J.A., 1990, *ApJ*, 351, L5
- Willick J.A., 1999, *ApJ*, 522, 647
- Willick J.A., Courteau S., Faber S.M., Burstein D., Dekel A., Strauss M.A., 1997, *ApJS*, 109, 333 (Mark III)
- Willick J.A., Strauss M.A., 1998, *ApJ*, 507, 64
- Worthey G., 1994, *ApJS*, 95, 107
- Zaroubi S., 2002, in Celnikier L., ed., *Frontiers of the Universe*
- Zaroubi S., Branchini E., Hoffman Y., da Costa L.N., 2002, *MNRAS*, 336, 1234
- Zehavi I., Riess A.G., Kirshner R.P., Dekel A., 1998, *ApJ*, 503, 483